Progress in Oceanography 229 (2024) 103365

Contents lists available at ScienceDirect

Progress in Oceanography

journal homepage: www.elsevier.com/locate/pocean

Extreme mismatch between phytoplankton and grazers during Arctic spring blooms and consequences for the pelagic food-web

Paul E. Renaud [a,b,1,*], Malin Daase [b,c,1], Eva Leu [a], Maxime Geoffroy [c,d], Sünnje Basedow [c], Mark Inall [e], Karley Campbell [c], Emilia Trudnowska [f], Einat Sandbank [d], Frida Cnossen [a], Muriel Dunn [a,d,g], Lionel Camus [a], Marie Porter [e], Magnus Aune [a], Rolf Gradinger [b]

[a] Akvaplan-niva, Tromsø, Norway
[b] The University Centre in Svalbard, Longyearbyen, Norway
[c] UiT The Arctic University of Norway, Tromsø, Norway
[d] Centre for Fisheries Ecosystems Research, Fisheries and Marine Institute of Memorial University of Newfoundland, St. John's, Canada
[e] The Scottish Association of Marine Science, Oban, UK
[f] Institute of Oceanology Polish Academy of Sciences (IOPAN), Sopot, Poland
[g] SINTEF Ocean, Trondheim, Norway

ARTICLE INFO

Keywords:
Arctic
Autonomous sampling technology
Energy flow
Pelagic ecosystem
Primary productivity
Sea ice

ABSTRACT

Food-web structure determines the cycling pathways and fate of new production in marine ecosystems. Herbivorous zooplankton populations are usually seasonally coupled with pelagic primary producers. Synchrony of phytoplankton blooms with reproduction, recruitment and seasonal ascent of their main grazers ensures efficient transfer of organic carbon to higher trophic levels, including commercially harvested species, especially in high-latitude systems. Changes in light, nutrient, and sea-ice dynamics due to accelerating climate change in the Arctic, however, create large uncertainties in how these systems will function in the future. To address such knowledge gaps, we surveyed the pelagic ecosystem of the Barents Sea Polar Front in May of two consecutive years (2021 and 2022) to investigate the pelagic food-web from primary producers to planktivorous fish. In both years we observed unprecedentedly high phytoplankton chlorophyll *a* values in open as well as ice-covered waters, much of which was invisible to satellite remote sensing. We also measured very low densities of grazing zooplankton across a wide area and extending for at least one month. This extreme mismatch resulted in low feeding by capelin, and further suggests a high potential for vertical export of carbon to the benthos rather than efficient assimilation into the pelagic food web. As the Arctic continues to warm and is characterized by thinner and more mobile sea ice, we may expect higher variability in phytoplankton bloom phenology and more frequent mismatches with grazer life-histories. This could have significant impacts on ecosystem functioning by redirecting the flow of energy through the system towards seafloor rather than to the production of commercially valuable pelagic marine resources.

1. Introduction

The flow of energy through marine ecosystems is governed by trophic interactions within the pelagic zone. The degree to which organic carbon (OC) produced during phytoplankton blooms is consumed by zooplankton determines in large part whether OC is channelled through pelagic or benthic food webs. Carbon pathways have strong implications both for carbon subsidies to higher predators, including commercially harvested species and marine mammals (Darnis et al. 2012), and the potential for carbon sequestration in marine sediments. A decisive link in this process is the coupling between primary production and grazing zooplankton. A 'match' scenario, when zooplankton abundances in the photic zone are high during a bloom period, favors retention of OC within the pelagic zone. In contrast a 'mismatch' between bloom peaks and high grazer density can result in high phytoplankton biomass accumulation and direct export of OC to deeper depth strata and,

* Corresponding author.
E-mail address: pr@akvaplan.niva.no (P.E. Renaud).
[1] These two authors contributed equally to the manuscript.

https://doi.org/10.1016/j.pocean.2024.103365

Available online 13 October 2024

eventually, the seafloor (Cushing 1990, Hunt et al. 2002, Dezutter et al. 2019).

Arctic marine ecosystems are characterized by a pulsed but intense spring bloom whereby half of the total annual new primary production can be generated within a few weeks (Wassmann et al. 1999, 2006). Stabilization of the water column by solar warming and/or sea-ice melt creates favorable growth conditions for phytoplankton, which flourish until nutrient supplies are exhausted, especially if grazing pressure is low. These surface blooms are iconic and visible in satellite imagery when occurring in open waters on clear days (e.g. Qu et al. 2005). Sea-ice algae also contribute to OC production early in the growing season, but depending on the amount of sea ice, they contribute up to only 16–22 % of the total annual primary production in the northern Barents Sea (Hegseth, 1998). The contribution of under-ice phytoplankton might increase in the future due to an increase in under-ice light availability caused by a climate-induced thinning of the sea-ice and/or increased period of open water (Ardyna et al., 2020). Grazing zooplankton, dominated in biomass by copepods of the genus *Calanus*, ascend from overwintering depths to feed on the bloom to fuel reproduction and to accumulate large lipid reserves for growth, development, and later overwintering, thereby performing a critical role in the transfer of bloom-derived organic carbon to higher trophic levels (Swalethorp et al. 2011). Developing copepods feed on microalgae and protozoans from the third naupliar stage, then are gradually more able to consume larger cells (and becoming more omnivorous later in summer/autumn) through their 5 copepodite stages. The level of coincidence of the bloom and the presence of grazing zooplankton (a 'match' scenario) has strong consequences for food-web dynamics and carbon cycling (Reigstad et al. 2011), not only in the pelagic but also benthic realm. The start of the spring phytoplankton bloom in the southwestern Barents Sea varies by over a month interannually (e.g., from around 10 April to 15 May) for the period 1998–2017 (Dalpadado et al., 2020). Population dynamics of Atlantic *Calanus* is also highly variable, and is affected by strength and timing of advection into the region (Głuchowska et al. 2017), local temperatures affecting copepod developmental rates (Skjoldal et al. 2021), and stock size of planktivorous fish (e.g. capelin, *Mallotus villosus*; Dalpadado et al. 2003). Reigstad et al. (2008) calculated that on average 36 % of PP is exported as POC to 90 m depth in the Barents Sea.

The Atlantic and Arctic regions of the Barents Sea are separated by a strong oceanographic front in the western half of the Sea. This Polar Front marks the approximate southern extent of winter sea-ice and is often an area of enhanced biological activity (Lien, 2018). The spring bloom in the southern Barents Sea usually begins in April or May and culminates in late May or early June (Tande 1991, Eiane and Tande, 2009, Oziel et al. 2017). Bloom timing has been observed to vary by several weeks, largely depending on latitude, seasonal ice cover, and melting regimes affecting water-column stability (Oziel et al. 2017, Makarevich et al. 2022). For example, the pelagic bloom maximum in the Atlantic Water regions of the Barents Sea occurs about 10–30 days before its occurrence in sub-Arctic and Arctic sections of the Barents Sea (de la Guardia et al. 2023). *Calanus* life-histories are thought to be well-timed to take advantage of the spring bloom and, along with grazing euphausiids, are efficient at channelling this energy to planktivorous fish such as capelin, herring (*Clupea harengus*), and polar cod (*Boreogadus saida*) (Kaartvedt, 2000; McNicholl et al. 2016).

Availability of zooplankton prey early in the season is critical to ensuring survival and growth of both juvenile and adult planktivorous fish. As they grow, both species consume meso- and macro- zooplankton, along with small fish and benthic organisms. These fish are also important forage species for numerous species of seabirds, marine mammals and piscivorous fish, including large commercial stocks of Atlantic cod (*Gadus morhua*) and haddock (*Melanogrammus aeglefinus*) (Dolgov 2002, Hop & Gjøsæter 2013, Planque et al. 2014).

In the Barents Sea, climate warming is expected to affect sea-ice distribution and seasonality, with potential impacts on water column stability and, thus, the timing of the spring bloom (Wassmann & Reigstad 2011, Oziel et al. 2017). Furthermore, an increased inflow of Atlantic Water and advection of nutrients, algae and fauna from the Norwegian Sea (i.e., an Atlantification of the region) have been observed in recent years (Edvardsen et al. 2003a, Edvardsen et al. 2003b, Orlova et al. 2015, Polyakov et al. 2017, Ingvaldsen et al. 2021). Earlier phytoplankton blooms and their mismatch with zooplankton have been observed occasionally in the southwest Barents Sea in years when early sea-ice melt leads to early stabilization of the water column (Eiane and Tande, 2009). More frequent occurrence of such a mismatch, along with altered community structure due to enhanced Atlantification, is likely to alter pelagic food-webs (Ji et al., 2013), with implications for carbon-cycling pathways in the water column and at the seafloor.

Research expeditions are valuable in documenting ecological processes, but observations often lack the temporal context with which to interpret the generality of cruise-based investigations. The enhanced access to satellite imagery and autonomous sampling platforms with integrated sensors can broaden the observational period to help provide increased context, both in time and space. The use of these technologies has already yielded interesting and novel results (e.g. Kahru et al. 2011, Basedow et al. 2019, Camus et al. 2021; Dunn et al. 2022), although deployment of autonomous platforms in the Arctic is not yet routine.

We conducted integrated studies of the pelagic ecosystem in late May in two consecutive years (2021, 2022), around the expected time of the spring phytoplankton bloom. Specifically, we investigated: (1) the phytoplankton bloom state along a longitudinal transect in the southwestern Barents Sea; (2) spatial overlap between phytoplankton and their zooplankton grazers; (3) the stomach fullness and diet of planktivorous fish in the region; and (4) spatial and temporal insights gained from the use of remote sensing technology. Observations are discussed in the context of consequences for energy flow and sustenance of commercial species.

2. Materials and methods

Cruises were conducted from 14 to 22 May 2021 and 18–27 May 2022 in the southwestern Barents Sea aboard the R/V *Helmer Hanssen* (Fig. 1). Sampling was performed during hydrographic transects, at fixed stations wheremultiple components of the pelagic ecosystem were sampled (Table 1, Supplementary Table T1), and from an autonomous Sailbuoy platform equipped with an EK80 wideband echosounder (16–260 kHz). The Sailbuoy collected acoustic backscatter data from 19 May – 15 July (2021) and 29 April – 24 July (2022), significantly expanding the temporal sampling window from the shipboard work and allowing for broader regional coverage outside the transect area.

This study was observational, aiming to assess the spatio-temporal match between phytoplankton and zooplankton grazers, and the implications of this, therefore we did not conduct explicit statistical analysis comparing e.g. the two years in question.

2.1. Hydrographic transects and sea ice

In 2021 and 2022, conductivity, temperature, depth (CTD; SBE911plus, Seabird Electronics Inc.) casts were conducted at stations along a section between approximately 75–77.5°N along the 29.5°E longitude line (Fig. 1). The CTD package measured conductivity, temperature, pressure, oxygen, fluorescence, turbidity and photosynthetically-active radiation (PAR), and was mounted on a frame that carried 12 5L-Niskin bottles for water sampling. Additional CTD casts were taken between the main stations to more clearly identify the location and structure of the Polar Front. In 2022, this strategy was augmented using a moving vessel profiler (MVP) when sea state and ice conditions allowed. The MVP is a winch that deploys a CTD (Applied Microsystems Ltd.) and other instruments as the ship steams at up to 7 knots, resulting in multiple sequential CTD and fluorescence profiles at approximately every 1 km.

Ice conditions were reported on a nearly daily basis by the

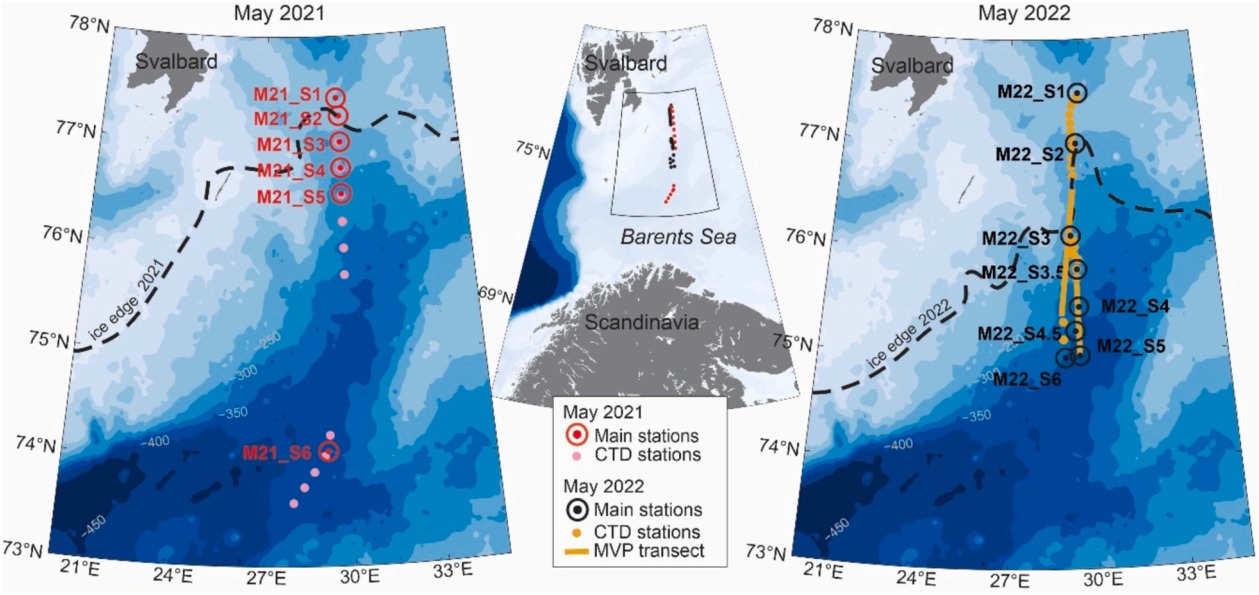

Fig. 1. Map of study area indicating main stations sampled in May 2021 (left) and 2022 (right) (M21-## and M22-##, respectively) and the ice edge during sampling in each year (dashed line). Additional CTD stations and MVP (moving vessel profiler) transect are also indicated by yellow dots and lines, respectively. (For interpretation of the references to color in this figure legend, the reader is referred to the web version of this article.)

Table 1
Overview of station locations (decimal degrees North and East latitude and longitude, respectively), bottom depth (m), and date sampled. Main stations are in bold text. Asterisks indicate stations where the ship had to move a short distance from the main station to trawl in open water. At four additional stations (not in bold), only the LISST was deployed. Depths where each sample was taken for the main parameters are presented in Supplementary Table T1.

Station	Latitude	Longitude	Bottom depth (m)	Date
M21_S1	77.42	29.92	200	17.05.2021
M21_S2	77.25	30	194	17.05.2021
M21_S3	77	30.02	238	18.05.2021
M21_S3*	76.88	30.12	251	18.05.2021
M21_S4	76.76	30.01	258	18.05.2021
M21_S5	76.51	29.99	287	19.05.2021
M21_S6	74.09	29.19	358	20.05.2021
M22_S1	77.5	29.85	196	24.05.2022
M22_S1.1	77.37	29.57	188	24.05.2022
M22_S1.2	77.21	29.51	203	24.05.2022
M22_S1.3	77.06	29.53	218	24.05.2022
M22_S2	77.03	29.53	229	25.05.2022
M22_S2*	76.99	29.76	233	25.05.2022
M22_S2.5	76.88	29.51	307	21.05.2022
M22_S3	76.15	29.38	282	21.05.2022
M22_S3*	75.98	29.52	306	21.05.2022
M22_S3.5	75.83	29.58	307	21.05.2022
M22_S4	75.48	29.63	353	22.05.2022
M22_S4.5	75.25	29.45	348	22.05.2022
M22_S5	75.01	29.51	371	19.05.2022
M22_S6	75	29.02	359	23.05.2022

Norwegian Meteorological Institute (https://cryo.met.no) and were used to optimize sampling plans. Stations south of 76°N were ice-free in both years whereby ice cover varied at other stations. We stopped the northward transect when ice conditions inhibited effective sampling (around 77.3°N in 2021 and 77.5°N in 2022). Sea ice was dynamic and some stations that were not accessible at the start of the cruise in 2022 were accessible and sampled one week later (Fig. 1).

The location of the Polar Front is usually defined as the zone of maximum sea-surface temperature (SST) gradient and/or southern extent of winter sea-ice (Lien, 2018). Thus, satellite-derived SST and sea-ice concentrations were downloaded from the freely available OSTIA (Operational Sea Surface Temperature and Ice Analysis) product (https://doi.org/10.1016/j.rse.2010.10.017). The best available cloud-free images closest in time to the CTD sections were from 4 May 2021 and 30 May 2022. Water masses were identified based on descriptions provided in Sundfjord et al. (2020) and are described in detail in Supplementary Material.

2.2. Chlorophyll *a* and phytoplankton community composition

Sea water for analysis of chlorophyll *a* (Chl *a*) concentrations was sampled from six depths (Supplementary Table T1) using Niskin bottles attached to a rosette carrying the CTD. Triplicate volumes of 250–1000 ml of seawater from each depth were filtered onto 25 mm GF/F filters (Whatman) and extracted in 90 % acetone overnight at 4 °C in the dark. The samples were then measured on board using a Turner Trilogy Fluorometer before and after addition of 5 % hydrochloric acid according to Parsons et al. (1984).

Phyto- and micro- plankton community analysis was performed on live samples onboard *Helmer Hansen*. At each station a 20 µm phytoplankton net sample (HydroBios, 0.125 m^2 opening) was taken from 30-20 m water depths to the surface. The sample was stored dark at 4° C until analysis. For microscopic analysis, the sample was thoroughly mixed and a small subsample (ca. 2.9 ml) was filled into an Utermöhl chamber and analysed alive within 1.5 h after sampling using a Zeiss Primovert inverted microscope. At least two sub-samples were analysed per station and typically the entire chamber was scanned for rare taxa.

2.3. Suspended particles

Vertical profiles of particle and phytoplankton distribution and abundance in the size range 3–500 um were assessed by Laser In-Situ Scattering and Transmissometry (LISST) were obtained at 11 stations to a maximum of 300 m depth to quantify suspended particle and phytoplankton concentration. The LISST-100X instrument is a laser diffraction device, and integrates optics for producing a collimated laser beam, a specially constructed detector array, electronics for signal pre-amplification and processing, data storage and scheduling computer, and a battery system. The principal measurement—angular scattering distribution—is obtained over 32 ring-detectors whose radii increase logarithmically.

2.4. Zooplankton sampling

Mesozooplankton was sampled by vertical hauls towed at 0.5 m s^{-1} from 10 m above the seafloor to the surface using a multiple opening/closing net (Multinet, Hydrobios, Kiel, mouth opening 0.25 m^2, mesh size 180 μm). Up to five depth strata were sampled at each location (Supplementary Table T1). Samples were preserved in a buffered 4 % formaldehyde-in-seawater solution. For species determination and enumeration, large (total length > 5 mm) organisms were removed from the entire sample, identified, and counted. The remaining part of the sample was examined by sub-sampling with aliquots obtained with 5 ml automatic pipette, with the pipette tip cut at 5 mm diameter to allow free collection of mesozooplankton. The number of subsamples analyzed was chosen so that at least 150 individuals of *Calanus* and 300 other copepods were counted. Samples with low abundance were examined in their entirety. Zooplankton abundance (ind. m^{-2}) was estimated by multiplying mouth-opening area assuming 100 % filtration efficiency. Abundance values were converted to biomass estimates in mg dry mass m^{-2} using species-specific dry mass as provided by Wold et al. (2023).

To estimate the abundance and biomass of macrozooplankton, a Tucker trawl (1500 μm mesh size, 1 m^2 opening) was towed for 15 min in the densest sound-scattering layer(s) (Supplementary Table T1) observed from the shipboard EK60 echosounder (18, 38, 120 kHz). The catch was sorted into taxonomic groups on board and all individuals of the larger functional groups (euphausiids, amphipods, chaetognaths, gelatinous taxa, jellies) were counted. The remaining mixture of copepods and smaller species (< 1 mm, i.e. mesozooplankton, analysed in detail in the multinet samples) was pooled and not identified. Abundances of macrozooplankton are presented as ind. m^{-3}. Sorted samples were placed in pre-weighed dishes and dried to constant mass at 50 °C to estimate dry weight. Abundance and biomass per m^{-3} were calculated by dividing count values by time trawled (s), vessel speed (m s^{-1}), and net opening area (m^2).

2.5. Pelagic fish sampling

Pelagic fish were only sampled during the 2022 cruise. This was performed using a Harstad pelagic trawl (80 m^2 opening at 3 knots, cod-end mesh size 5.5 mm). At each station, the trawl was towed at ca. 3 knots for 20–30 min in the densest sound scattering layer, similar to the Tucker Trawl described above. Trawl catch was sorted and identified to genus or species level on board. Standard length and weight of planktivorous capelin and polar cod were measured from a sub-sample, and stomachs were extracted from these fish. Stomach contents from 30 fish of each station-dependent size class (capelin: small: 6–9 cm, medium: 8–12 cm, large > 12 cm; polar cod: one size class: 9–19 cm) were identified under a stereomicroscope to broad taxonomic groups, and stomach fullness, number of individual prey items present, and the volumetric percentage composition for each prey item were recorded.

Shipboard acoustic surveys: The keel-mounted Simrad EK60® split-beam echosounder from the *Helmer Hanssen* continuously recorded hydroacoustic data at 18, 38, and 120 kHz. The ping rate was set to 1 s and pulse length to1,024 μs. The echosounder was calibrated annually using the standard sphere method (Demer et al. 2015). Temperature and conductivity profiles from the CTD were used to compute sound-speed profiles (Chen & Millero 1977) and the coefficient of absorption at each frequency for each region (Francois and Garrison 1982).

Shipboard acoustic data along the cruise tracks from 2021 and 2022 were quality-controlled and cleaned with Echoview® v. 13 and 14. We used Echoview's algorithms to remove background noise, impulse noise, and attenuated noise signals (De Robertis and Higginbottom 2007; Ryan et al. 2015). A minimum signal to noise ratio threshold of 10 dB was applied. Samples with a lower signal to noise ratio were considered indistinguishable from background noise and were excluded from the analysis with the background noise algorithm. In both 2021 and 2022 pelagic capelin schools, validated with a midwater trawl, were concentrated in the upper 200 m. We ran Echoview's school-detection algorithm within that region on the 38 kHz echogram, the frequency generally used for swim-bladdered pelagic fish detection, to isolate capelin schools (parameters in Supplementary Table T2). Proportion of capelin in detected schools as well as average fish lengths were calculated using the closest pelagic trawl catches. To calculate capelin volumetric density in fish m^{-3}, the average volume backscattering strength (S_v in dB re 1 m^{-1}) at 38 kHz within each capelin school was divided by the Target Strength (TS in dB re 1 m^{-2}) of the average capelin. TS was calculated based on the average length of capelin in the net samples and using a relationship between TS and length (L) for capelin in the Barents Sea (eq. (1); Toresen et al. 1998):

$$TS = 19.1 * log(L) - 74.0 \quad (1)$$

No individual weights of capelin were collected in 2021, thus biomass estimates are based on the length to weight relationship for capelin (eqn. (2); from Froese et al. (2014)):

$$W = 0.00363 x L^{3.21} \quad (2)$$

To calculate biomass of capelin (g m^{-3}), the density obtained from acoustic signal processing was then multiplied by the average weight of capelin caught in the trawl. Calculations were conducted in the linear domain.

Autonomous acoustic surveys: The autonomous hydroacoustic surveys were completed using a Sailbuoy (Offshore Sensing AS) equipped with an EK80 WBT Mini transceiver (Kongsberg Maritime AS) and a 200 kHz transducer (ES200-7CDK split-beam) mounted on the keel. Data collection parameters for each mission are summarized in Supplementary Table T3. The Sailbuoy was piloted from land. Areas with sea ice were avoided, thus limiting data collection from the northern part of the study region at the same time as the ship was present. However, the autonomous surface vehicle extended the sampling footprint after the ship was in the area, allowing shipboard data to be placed in a broader temporal and regional context.

The echosounder mounted on the Sailbuoy was calibrated before the 2021 mission on 21 April 2021 using the standard-sphere procedure (Demer et al., 2015). The calibration parameters were calculated using the EK80 calibration wizard (version 2.0.1, EK80 software, Kongsberg Maritime AS, Horton, Norway). Acoustic data were pre-processed and noise-removal algorithms were applied to the nominal frequency (200 kHz) for both Sailbuoy acoustic datasets following the same method as the shipboard acoustic data analysis. The backscatter signal from bubbles and entrained air below the surface was removed using a maximum threshold line. The volume backscatter was depth-integrated between the entrained-air line and 50 m range. These processing steps were worked into a pipeline that was applied to all files in the dataset for each year using Echoview scripting with Python (version 3.7). The frequency of the Sailbuoy-mounted echosounder allows detecting macro- and mesozooplankton. The volume backscatter from the epipelagic layer (surface − 50 m) as measured from the Sailbuoy is therefore used as an indication of relative zooplankton abundance over the sampling area.

3. Results

3.1. Ice conditions and hydrography

In both years our study region was dominated by Polar Water (north of the Polar Front) and warm Polar Water south of the Front, with Atlantic Water at the southernmost station (Fig. 2, Supplementary Figures S1-S3). In May 2021, the surface front along our transect was strongest at around 76.5° N, close to the edge of the marginal ice zone (MIZ: defined as at sea ice concentration = 0 %; Supplementary Figure S4c). The Polar Front on 30° E exhibited a wedge-like structure with subsurface horizontal temperature gradients increasing with depth and towards the north (Fig. 2). Thus, warmer waters extended

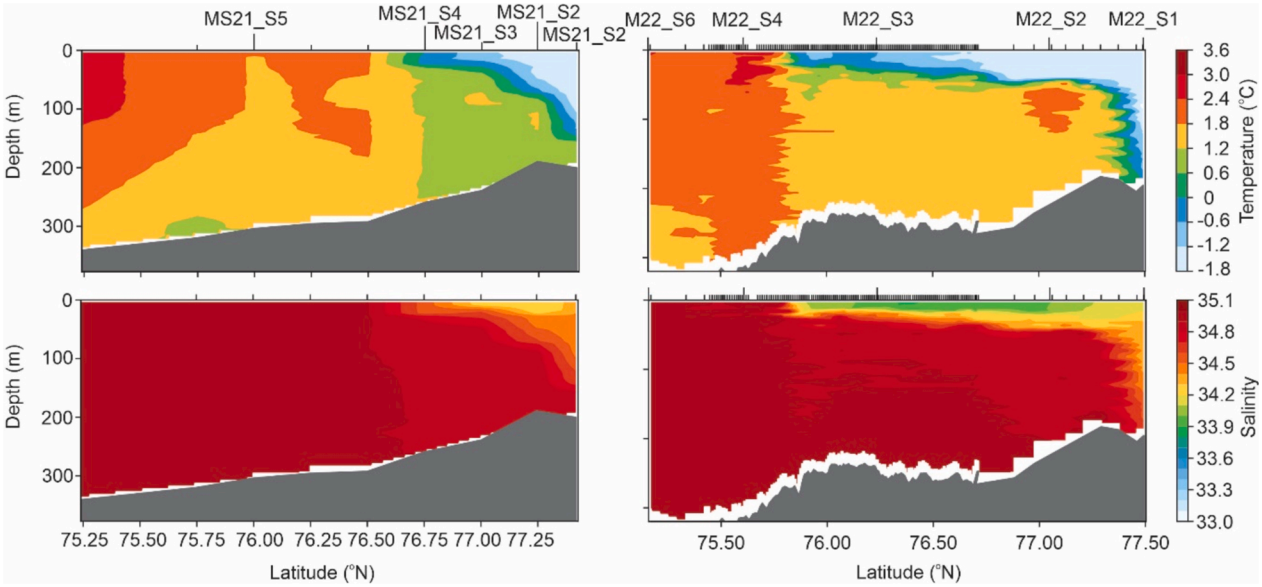

Fig. 2. Spatial variability in temperature (upper panels) and salinity (lower panels) along station transects from South (left in panels) to North (right in panels), x-axis is latitude (°N), in May 2021 (left panels) and May 2022 (right panels). Dark grey areas indicate seafloor depth.

northward of the surface front by more than 100 km. The highest temperature gradient was found at ~ 100 m depth at ~ 77.3° N, likely a consequence of strongest water mass convergence (Supplementary Figure S4a, b).

In May 2022 the surface front was more diffuse between 75.5° and 76.75° N, but with subsurface horizontal temperature gradients much sharper than in 2021. The temperature section alone makes defining the location of surface expression of the front ambiguous. However, fractional analysis of water masses indicated that surface waters are found to consist of > 50 % Polar Water as far south as 75.75° N (Supplementary figure S3d, e). Thus, it seems reasonable to say that the surface expression of the front was located at 75.75° N on 29.3° E in May 2022. Vertically, it exhibited a much more step-like structure than in 2021 with a patch of relatively warm water (1.5 °C) centred around 75 m at 77.2° N (Fig. 2).

3.2. Phytoplankton Chl *a* concentrations, and bloom state

In 2021, Chl *a* concentrations at the three northernmost stations (M21_S1-S3) in stratified waters peaked in the uppermost 15–25 m and reached a maximum of 22 mg m^{-3} at M21_S1 (Fig. 3). At station M21_S4, the Chl *a* peak was slightly deeper (between 20 and 50 m), and higher concentrations (> 5 mg m^{-3}) extended to 100 m. At the two southernmost stations with mixed water columns (M21_S5-S6), Chl *a* concentrations were more evenly distributed throughout the entire water column and reached maxima of 15–20 mg m^{-3} (Fig. 3). Depth-integrated Chl *a* was high at all stations in 2021 (Fig. 4a), peaking at M21_S5 (1600 mg m^{-2}), and values at other stations ranging from 565-1300 mg m^{-2} (Fig. 4a).

In 2022, vertical profiles of Chl *a* were similar to 2021, with pronounced peaks occurring between 10 and 30 m at M22_S1-S3, and slightly deeper at M22_S4. The highest Chl *a* concentrations were observed at M22_S4 (18.6 mg m^{-2}) at 20 m. In contrast to May 2021, Chl *a* concentrations below 100 m depth were low at all stations (Fig. 3). Depth-integrated Chl *a* was lower in May 2022 than in May 2021 (ranging from 155 to 740 mg m^{-2}), with the highest values at M22_S3 and M22_S4 (Fig. 4a).

The phytoplankton community in both 2021 and 2022 was dominated by centric diatoms characteristic of an Arctic spring-bloom (Table 2), including several *Thalassiosira* spp. (mainly *Thalassiosira antarctica* var *borealis*) and *Chaetoceros gelidus*. Additionally, *Phaeocystis pouchetii* contributed to various extents at all stations, but in a secondary manner. Heterotrophic dinoflagellates of the genera *Gyrodinium* and *Protoperidinium* occurred at all stations, while ciliates were rarely seen. In May 2021, all samples were dominated by centric diatoms. At the northernmost stations (M21_S1 to M21_S3), a larger fraction of diatoms had already formed resting spores, indicating a later successional stage, and *Phaeocystis pouchetii* and *Chaetoceros gelidus* dominated. At the southernmost stations other *Chaetoceros* and *Thalassiosira* species dominated (without resting spores), while *P. pouchetii* and *C. gelidus* occurred only rarely. In May 2022, the phytoplankton community of the ice-covered northernmost stations were characterized by the presence of several typical Arctic ice algal taxa in the water column (including *Nitzschia frigida)* in addition to phytoplankton bloom species, while *Phaeocystis pouchetii* was not observed. At one station (M22_S5), the colonial choanoflagellate *Parvicorbicula socialis* was moderately abundant, but it was not observed at any of the other stations. Resting spore formation was not observed in May 2022.

The concentration of suspended particles as identified by the LISST in 2022 was low at the Arctic side of the Polar Front, as well as at the two southernmost Atlantic Water-dominated stations, while high concentrations were observed at several stations located within the Polar Front region (Fig. 4c).

3.3. Zooplankton communities

At main stations along the transect (MS21_S1-S5) in 2021, mesozooplankton abundance varied between 56,500 ind. m^{-2} (MS21-S2) and 167,500 ind. m^{-2} (MS21_S5) (Fig. 4b). At the southern station M21-S6 total abundance was > 5 times higher (930,000 ind. m^{-2}). The mesozooplankton community was dominated by small copepods (adults size < 1.5 mm, mainly *Oithona similis*) accounting for 56 % and 66 % of the total abundance at the northern stations (M21_S1 and S2), for ca. 30 % at M21_S3-5, but only for 12 % at MS21_S6 where copepod nauplii and appendicularians made up a large proportion of the community (27 and 30 %, respectively, Fig. 3b). Ahigh contribution of copepod nauplii was also observed at M21_S5 (40 % of total abundance). Abundance of the large herbivorous copepods of the genus *Calanus* was rather low along the transect (3480–9780 ind. m^{-2}), where they only contributed 5–10 % to the total mesozooplankton community. Higher abundance and contribution of *Calanus* spp. was only observed at M21_S6 (179,600 ind. m^{-2}, 19 % of total abundance). At the northern stations (M21_S1 &2),

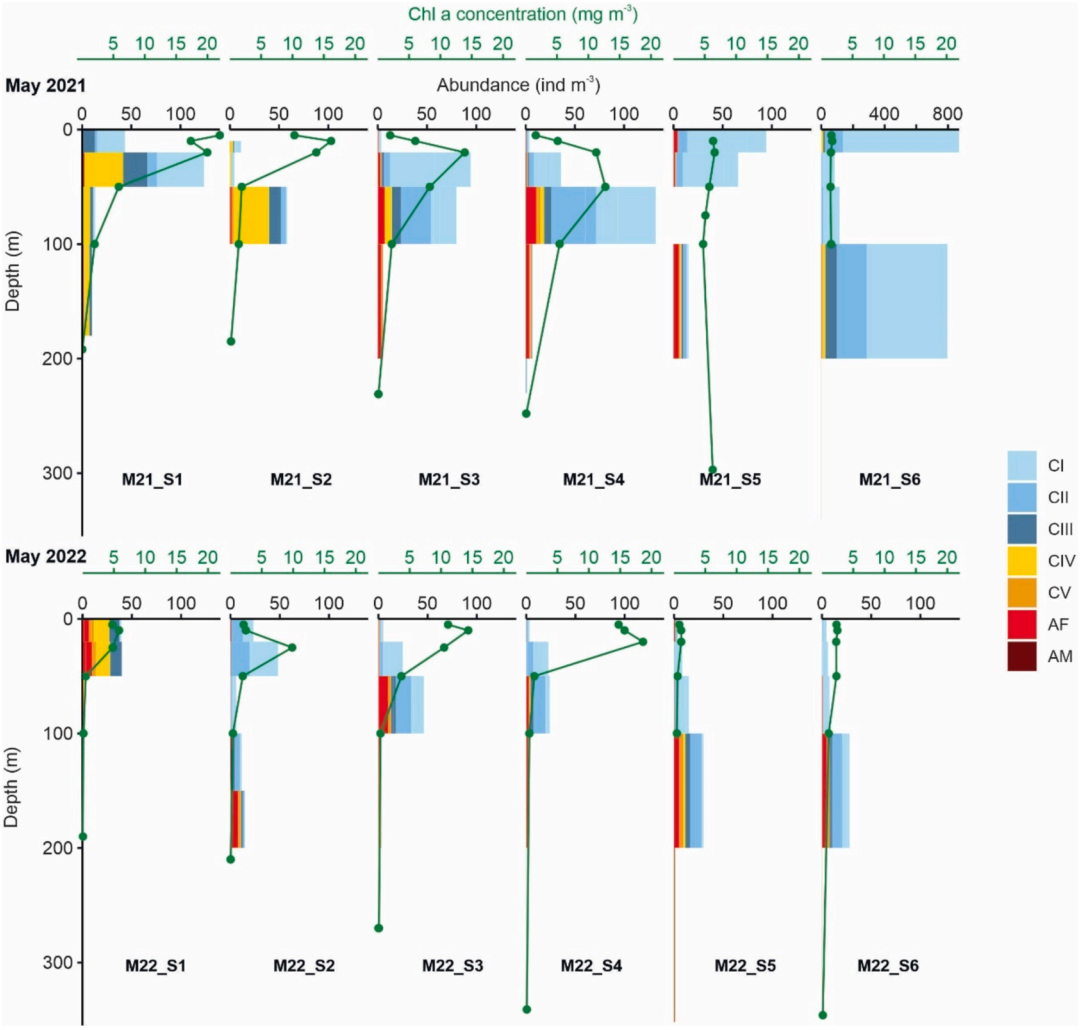

Fig. 3. Vertical distribution of Chl *a* concentration (green lines, upper scale bars) and *Calanus* spp. abundance and stage composition (colored bars, black scale) in May 2021 (upper panel) and May 2022 (lower panel). Note differences in scale of x-axis for *Calanus* abundance for M21_S6. Stage compositions indicated include five copepodite stages (CI-CV) and adult female and male (AF, AM). (For interpretation of the references to color in this figure legend, the reader is referred to the web version of this article.)

the *Calanus* population consisted mainly of copepodite stages CIII and CIV (54—78 %). At MS21_S1, we also found a high contribution of CIs (34 %). Early copepodites stages CI and CII also dominated the *Calanus* population at stations M21_S3-S5 (~75 %) and M21_S6 (90 %) (Fig. 3). At M21_S3-5, adult females accounted for ~ 11 % of the population, otherwise adults and older overwintering stages (CV) were rare at all stations. *Calanus* abundance peaked between 20–100 m (Fig. 3) at most stations, with low abundance below 100 m, except for M21_S5 where abundance of CI peaked in the surface layer, and a bimodal distribution with peaks in abundance (mainly CI) in 20–0 m and 100–200 m at M21_S6 was observed (Fig. 3).

Mesozooplankton abundance was slightly higher in May 2022 than in May 2021. Highest abundance was observed at the northernmost stations, reaching 253,200 and 346,600 ind. m^{-2} at M22_S1 and S2, respectively. Lowest zooplankton abundance was observed at M22_S3.5 in the central section of the transect (103,000 ind. m^{-2}). Small copepods dominated the community at most stations (62 % of the total abundance at MS22_S1, 35–40 % at the other stations). Appendicularia were abundant in the northern end of the transect, while benthic larvae (meroplankton) accounted for 20–40 % of the mesozooplankton community south of 76° N (Fig. 3). Similar to May 2021, *Calanus* abundance was low (3620–7500 ind. m^{-2}) in May 2022, contributing < 3.2 % to the total mesozooplankton abundance at all stations except for M22_S3.5 (7 %). The *Calanus* population consisted mainly of young copepodites (CI-CII) (55–74 %), except for the northernmost stations where CIII-CIVs dominated (65 %). Adult females accounted for 12–22 % of the population along the transect, while CIII-CVs were rare. *Calanus* abundance peaked below 100 m at the southernmost stations (S5 and 6), in 50–100 m in the middle section of the transect and in the upper 50 m at the two northernmost stations (Fig. 3).

The macrozooplankton community was dominated by chaetognaths and euphausiids, but overall abundance and biomass were very low (Fig. 4d, Supplementary Table T5). Highest abundances of chaetognaths were found at the southern end of the transect in 2022. A higher proportion of euphausiids was observed at the ice edge/Polar Front region in both years. Species composition of both meso- and macrozooplankton communities indicated a mixture of Arctic and boreal taxa, which is common for the region throughout the year. The larger *Calanus* found at the northernmost stations were identified as the Arctic *C. glacialis* based on prosome length, but we did not carry out the molecular analysis to confirm this.

Acoustic surveys by the Sailbuoy deployments extended our observations of zooplankton communities at main stations by several weeks to 2 months in 2021 and 2022. In 2021, the Sailbuoy was deployed at the southern end of the transect but sea ice and strong winds prevented many passages across the Polar Front until after June. The acoustics

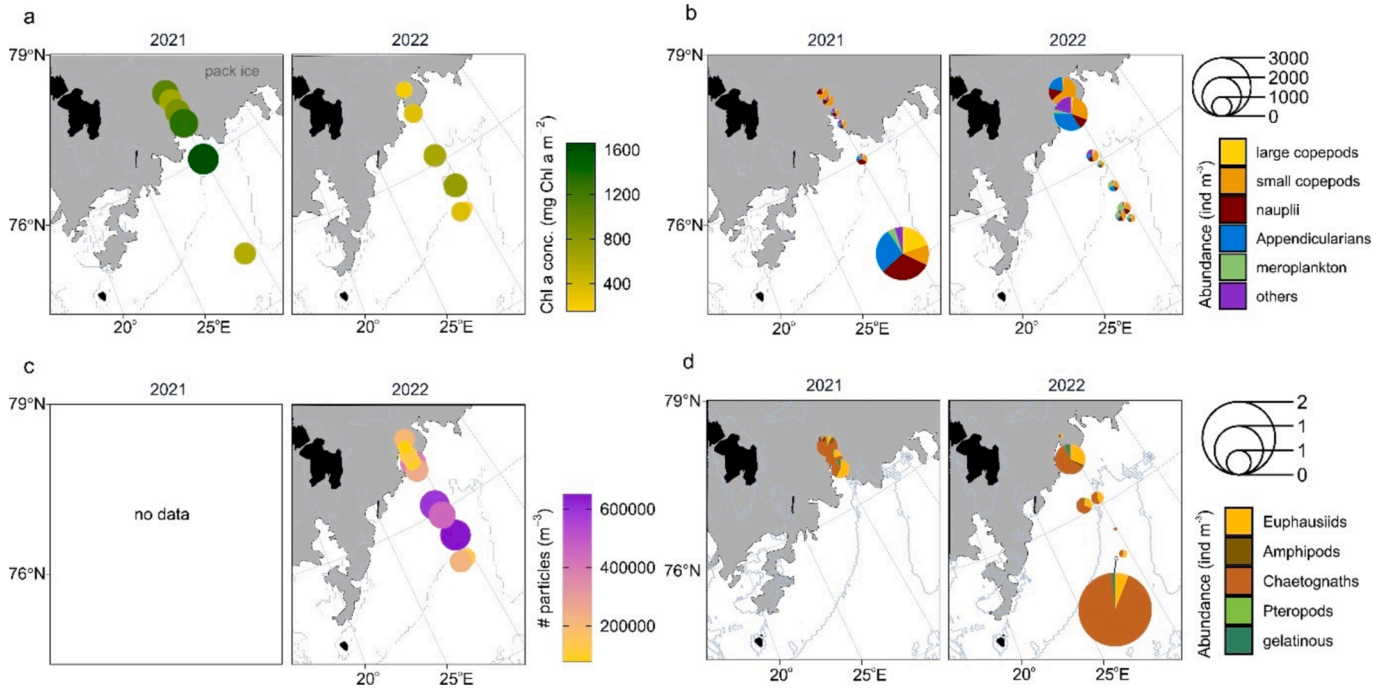

Fig. 4. Spatial distribution of (a) depth-integrated Chl *a* concentration; (b) mesozooplankton species composition and abundance (integrated over water column); (c) number of particles (integrated over upper 100 m); and (d) species composition and abundance of macrozooplankton in sound scattering layers. Size of data points in (b) and (d) reflect total densities. The light grey area shows region that was ice covered. No LISST data were collected in 2021.

Table 2
Dominant phytoplankton taxa identified at the main stations in 2021 and 2022.

	Thalassiosira antarctica v *borealis*	*Thalassiosira nordenskiöldii*	*Chaetoceros gelidus*	*Entomoneis* sp.	*Nitzschia frigida*	*Phaeocystis pouchetii*	*Gymnodinium* sp.
2021							
M21_S1	x		x			x	x
M21_S2	x					x	x
M21_S3	x	x	x			x	x
M21_S4	x		x				x
M21_S5	x		x			x	
M21_S5	x		x			x	x
M21_S6	x		x				x
2022							
M22_S1	x		x		x		x
M22_S2	x		x	x	x		
M22_S3	x		x			x	
M22_S4	x	x	x			x	
M22_S5	x		x			x	
M22_S6	x	x	x				x

detected moderate amounts of zooplankton backscatter south of 75.5°N but very low backscatter was detected in the study region closer to the Polar Front until July. Similarly in 2022, (uncalibrated) backscatter values north of 75.7° N were low in several transects across the Front from mid-May until late June when the Sailbuoy left the region (Fig. 5).

3.4. Capelin abundance and diet

In both years, capelin schools primarily occupied the upper 200 m of the water (Supplementary Figure S5). Due to the water temperature and salinity gradient the transect was divided into two regions, based on the latitude where water temperature and salinity started to rapidly change. In 2021 this boundary was set at 76.75° N. Schooling capelin were observed consistently along the survey transect south of 76.75N. North of 76.75° N, capelin schools were larger, more dispersed, and observed at a lower frequency (Fig. 6). In the northern region, the average volumetric density within the schools reached 0.13 fish m^{-3} (sd = 0.12) with the average height of the schools reaching 13.02 m (sd = 10.50). South of 76.75N, capelin density within schools reached 0.68 fish m^{-3} (sd = 0.41) with an average fish school height of 6.80 m (sd = 3.11 m) (Supplementary Table T5). The overall density along the transect was 0.63 fish m^{-3} (sd = 0.42) and the overall average school height was 7.31 m (sd = 4.54).

North and south regions in 2022 were divided at 75.9° N, and parameters of school density, biomass and height were similar to those estimated in 2021 (Supplementary Table T5). Again, schools were denser and had both higher biomass and school height in the southern region (Fig. 6), although values for all parameters were slightly lower in the southern region and higher in the northern region than in 2021 (Supplementary Table T6).

Capelin density estimates calculated from the acoustic trawl surveys are likely conservative. We assumed that the species composition within the closest pelagic trawl sample was representative of the composition within the school. However, pelagic fish generally, but not always, form

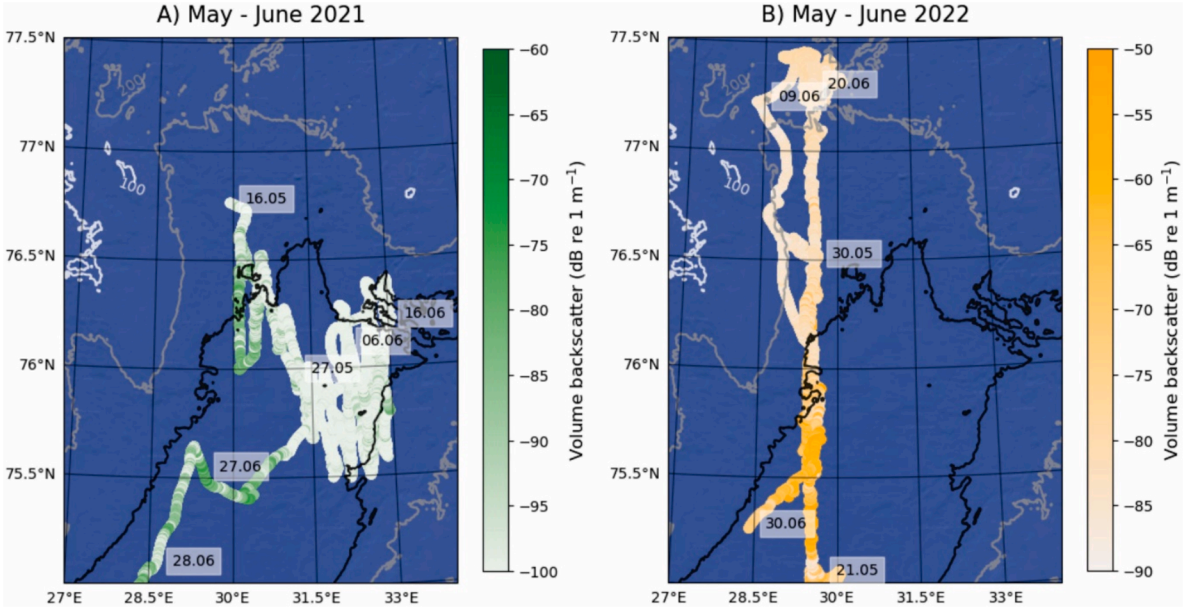

Fig. 5. Temporal variability in acoustic backscatter recorded by Sailbuoy in the study area for two months following the field campaign in 2021 (left) and 2022 (right). Backscatter in 2022 was not calibrated but the relative values of the two plots are comparable within each year. Dates are indicated along the transect paths. White, grey, and black lines represent bathymetry (100 m, 200 m, and 300 m, respectively).

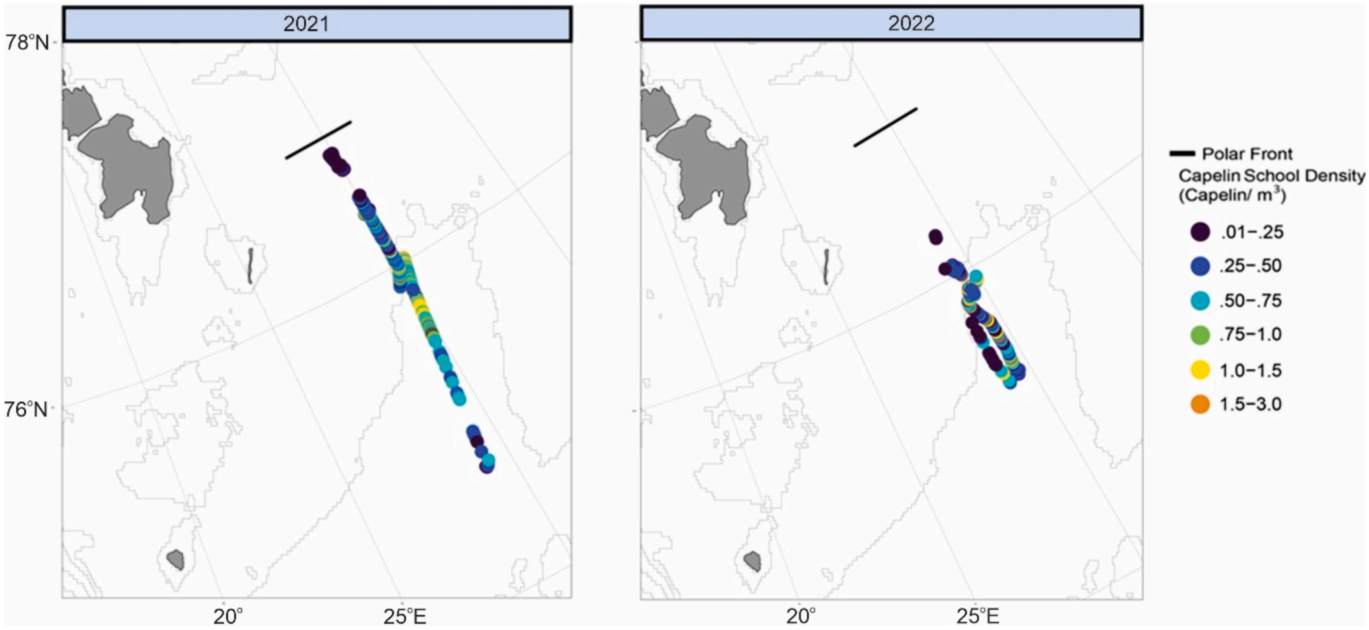

Fig. 6. Map indicating densities of capelin schools estimated from the shipboard EK60 within the upper 200 m along transects in 2021 (left panel) and 2022 (right panel). Color indicates calculated average capelin density (fish m^{-3}). Plotted fish school locations are based on the coordinates where the maximum school backscatter value was measured. Estimated location of the surface Polar Front, based on CTD salinity and temperature interpolation, is indicated by the solid line.

monospecific schools (Lawson et al. 2001). Because it is unknown if the two most abundant species, capelin and polar cod, segregate or mix when schooling near the surface we decided to apply the ratio of capelin sampled in the nets to our density calculations.

Stomach content analysis indicated that capelin were not feeding or feeding only at low levels in May 2022 (mean fullness < 10 %, Fig. 7) at all stations except the northernmost trawling station M22_S2*. Capelin from most of the stations were caught at depths where macrozooplankton did not occur in high abundances. Larger capelin caught at M22_S2* had mean fullness of 40–60 %, indicating that they were feeding. Polar cod, when caught either north or south of the Polar Front, were feeding at much higher levels and were caught at depths with higher macrozooplankton abundance. No polar cod were found with empty stomachs. The main prey items for both fish species were euphausiids and copepods, making up well over 80 % of identifiable prey (Fig. 7). Fish comprised 10–15 % of identifiable prey found in polar cod stomachs.

4. Discussion

We recorded exceptionally high concentrations of Chl *a* during May in the two consecutive sampling years. A combination of favourable

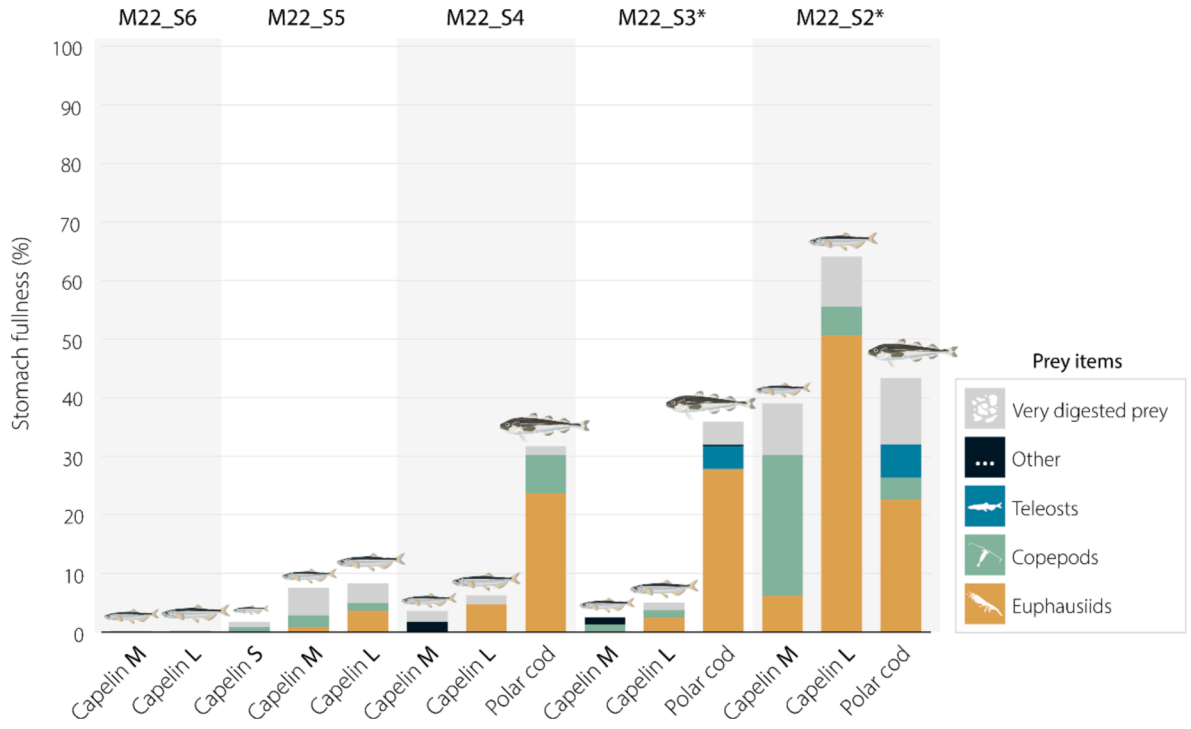

Fig. 7. Mean stomach fullness (%) and taxonomic composition of stomach contents in capelin (S = small, M = medium, L = large) and polar cod from stations sampled in May 2022. Asterisk indicates that two trawling stations were taken nearby main stations but not at exactly the same location (due to sea ice). See Table 1.

growth conditions in terms of light and stratification, alongside a lack of top-down control due to very low abundances of grazing zooplankton appeared to be key factors explaining such levels of algal biomass. These findings contradict the conceptual match-based model of bloom development and trophic connectivity and bring into question satellite-based observations of phytoplankton bloom magnitude for the region. Such a high abundance of phytoplankton without abundant consumers has strong implications for the maintenance of a vital pelagic ecosystem in a region where zooplankton and planktivorous fish are the primary food resources for commercially harvested fish species.

4.1. *Phytoplankton bloom state*

Despite substantial sea-ice cover, Chl *a* concentrations observed during both May 2021 and 2022 were two to four times greater than previously reported concentrations for the Barents Sea, reaching a maximum of 22 mg m^{-3} and most stations exhibiting values over 5 mg m^{-3} (Fig. 2). A recent empirical study in the same area during May 2016, 2018, and 2019 documented values only up to1–5 mg m^{-3} (Makarevich et al. 2022) and a combined remote sensing/modelling study estimated values approximately one order of magnitude below our maximum values (de la Guardia et al. 2023). The timing of sampling may contribute to this difference in that bloom phenology could change considerably in 1–2 weeks. The Makarevich et al. (2022) values are already high for the region, however, and we argue that bloom conditions were different during our study.

At all stations, typical spring bloom phytoplankton composition was encountered with slight differences. Diatom taxa that dominated at most stations (*Thalassiosira* spp. and *Chaetoceros* spp.) are typical for early stages the Barents Sea spring bloom (Wassmann et al. 1999, 2006). In addition, ice-algal taxa found in some northern stations and late-bloom indicators, such as *Phaeocyctis pouchetii*, indicate that the onset of the bloom differed in timing across the transect and between the two years with local inputs from sea ice. All stations exhibited high integrated Chl *a* values, exceeding 1000 mg m^{-2} at several stations due to high concentrations under conditions below 100 or even 200 m depth at the weakly or non-stratified southerly stations.

Ice cover (and snow on ice) can control the timing of the Arctic pelagic phytoplankton blooms by affecting light availability with thin ice and snow, as well as leads (all observed both years in this study), limiting inhibitory effects on algal growth. These observations are in line with the general trend of under-ice phytoplankton blooms becoming more wide-spread and representing a larger part of the annual new production as a consequence of ongoing climate warming (Ardyna et al. 2020, and references therein). Under-ice blooms have been documented since the 1950 s under sea-ice, and these blooms can reduce concentrations of inorganic macronutrients like nitrate and silicate (Balch et al. 2014), resulting in nutrient-depleted surface waters and deep Chl *a* maxima immediately after seasonal ice retreat (Oziel et al. 2019). Thus, open-water pelagic primary productivity later in the season will likely be reduced in areas where under-ice blooms have been extensive.

Melting sea ice can stabilize surface waters and help to initiate a phytoplankton bloom, as suggested in the Sverdrup critical-depth hypothesis (Sverdrup 1953). The conceptual model for marginal ice zone blooms suggests a northward-migrating phytoplankton bloom as the ice edge retreats in the spring (Wassmann et al. 2006). However, this paradigm seems to be weakened under current and future conditions with earlier onset of the blooms developing under thinner sea-ice (Oziel et al. 2019). We found melt-water layers of varying thickness under the sea ice, and this was particularly obvious in salinity profiles south of the surface Polar Front where it appeared ice had been advected from the north and begun to melt (Fig. 2). A cruise that visited the same area just two weeks prior to our sampling in 2021, however, observed bloom initiation without surface-water stratification (Koenig et al. 2023). That study (Koenig et al. 2023) found integrated Chl *a* values of around 100 mg m^{-2}, while just two weeks later we recorded values of 1600 mg m^{-2}, indicating rapid bloom development. A modelling study investigating the role of sea-surface temperature and ice cover in bloom formation in the Barents Sea found little consistent relationship but suggested that the bloom occurs before or immediately following ice retreat when retreat is late (after mid-May) (Dong et al. 2020). Our observations are consistent with this result, but we have no unequivocal evidence for the mechanism

behind our observations.

The Barents Sea Polar Front is a stable feature where warmer Atlantic Water meets colder Arctic Water masses, and often marks the southern extent of winter sea-ice. Lien (2018) suggested that the 'passive' nature of the Front probably does not contribute to enhanced primary production, but its physical structure may lead to aggregation of different species at some times of the year. Data from LISST deployments support this latter suggestion, as they indicate an accumulation of particles in the stations adjacent to the Front. The accumulations of the small particles at the Polar Front were observed earlier on the west Spitsbergen shelf (Trudnowska et al. 2016). As they are linked to elevated Chl *a* concentrations, these particles were likely phytoplankton cells. It may well be that the Polar Front does not lead to enhanced primary productivity via dynamic mixing as observed at other frontal systems, but the interaction of the warmer Atlantic Water mass with sea ice advected southward is likely to contribute to bloom initiation via the processes discussed above.

4.2. Match/mismatch scenario

Initiation of phytoplankton blooms due to adequate light and nutrient conditions does not in itself explain the unprecedented high Chl *a* concentrations we observed. While there is often a lag between phytoplankton growth and grazer pressures resulting in greater phytoplankton abundances, it is clear in our study that the very high levels of phytoplankton biomass were only possible due to an extended period of low zooplankton abundances, representing an extreme mismatch between primary productivity and grazing pressure.

In both years, we observed mesozooplankton abundances (mean 105,100 and 203,300 ind. m^{-2} in May 2021 and 2022, respectively) and biomass values (mean 1216 and 2044 mg dry mass m^{-2} in May 2021 and 2022, respectively) that were very low compared with observations from summer and late autumn in the western Barents Sea (Wold et al. 2023). Our abundance estimates from May 2021 and 2022 were comparable to estimates made by Wold et al. (2023) south and north of our study area (222,500 and 196,900 ind. m^{-2} and 1411 and 1113 mg DM m^{-2} respectively), just two weeks prior to our sampling in 2021. In that study, samples were also dominated by juvenile stages of copepods. Similar low abundances have previously been observed in May in different Svalbard fjords (e.g. Daase and Søreide, 2021, Søreide et al., 2022) and at the Barents Sea Polar Front in May 1999 (Blachowiak-Samolyk, 2008), but these observations were generally made prior to the spring bloom. Wold et al. (2023) document a pronounced seasonality in mesozooplankton abundance in our study area, with a substantial increase in abundance between spring and summer, and peaks in later summer and autumn. Such a pronounced seasonality in mesozooplankton community structure has also been observed in Svalbard fjords (Walkusz et al. 2009, Søreide et al., 2022) and elsewhere in the Arctic (Madsen et al. 2001, Ashjian et al. 2003, Darnis and Fortier 2014) and subarctic (Tande 1991, Coguiec et al., 2023), but seasonal variation was not observed in the Barents Sea in 1998–1999 (Arashkevich et al. 2002).

In addition to the low mesozooplankton abundance, we also observed very low abundance of macrozooplankton (mean of 0.4–0.5 ind. m^{-3} in both years). Macrozooplankton, and euphausiids in particular, are known to be generalist feeders but are important herbivores during spring blooms (Falk-Petersen et al. 2000, Dalpadado et al. 2008, Huenerlage et al. 2016). Their abundance is notoriously difficult to assess as they are fast swimming and able to avoid nets, even when nets are trawled horizontally, and comparison of our data with previous studies is difficult. We selected our sampling depth based on sound scattering layers on the echosounder, but even within these layers the backscatter was generally weak, which was reflected in the corresponding low catch. The acoustic surveys we conducted using a Sailbuoy during and for some weeks after the end of our cruise are expected to have reliably assessed macrozooplankton assemblages as acoustics does not trigger avoidance behavior. The results confirm that both mesoandmacrozooplankton abundances were low in the wider area and lasted for at least a month. This strongly suggests that our observations were representative and relevant for describing the ecosystem status in May-June of both years.

The low abundance of larger grazers (*Calanus* spp. and *Thysanoessa inermis*) in the upper pelagic layer stands out. Young copepodites (CI-CII) capable of grazing phytoplankton were found in our study (but were almost absent two weeks prior to our sampling (Wold et al. 2023)), and this may be viewed, from the copepod perspective, as matching reproduction to the phytoplankton bloom. But abundances were low (see above) and combined with the lack of larger life stages, total grazing pressure was clearly very low. Thus, it is plausible to assume that the extraordinary levels of Chl *a* observed in this study resulted from a lack of efficient top-down control of phytoplankton by grazing.

The mechanisms causing these low abundances of mesozooplankton, and large grazers in particular, during these two consecutive spring-bloom periods remains unclear. At least three non-exclusive explanations can be suggested to explain the extreme mismatch of grazing zooplankton with the pelagic phytoplankton blooms observed. First, top-down processes (predation by macrozooplankton and fish) may lead to sharp declines in overwintering zooplankton populations. The southern Barents Sea is a winter spawning area for a large proportion of the Barents Sea capelin population, and the relatively warm waters may also be a winter refuge for other fish species. Juvenile redfish (*Sebastes* spp.) were abundant at our southernmost sampling locations during both years, as were juvenile haddock (*Melanogrammus aeglefinus*) (Cnossen 2022). And while the macrozooplankton abundance was overall low, the community was dominated by chaetognaths which also prey on copepods and could have had significant predation pressure on the copepod community (Samemoto, 1987, Terazaki 2004).

Second, non-consumptive mortality of copepods may deplete the stocks of overwintering copepods. Wold et al. (2023) report low mesozooplankton abundance in the study area already in March 2021 compared to observations from December 2019, suggesting high winter mortality. In a study covering both Svalbard fjords and open Arctic slope regions, Daase et al. (2014) found that 9–94 % of *Calanus* spp. collected at depth were dead. The authors suggested that limited energy resources, parasitism, or adverse environmental conditions were responsible for high mortality rates. In our study, approximately 8 % of *Calanus* spp. collected in May 2022 were dead, suggesting low non-consumptive mortality at that time (M. Daase, pers. observation). One contributing factor to non-consumptive mortality is death after reproduction, which is common in most copepods. The dominance of early copepodite stages and high contribution of copepod nauplii in both years indicate that reproduction had occurred prior to our sampling campaign. Most of these young life stages fell into the size range assigned to the Arctic *Calanus* species (*C. glacialis* and *C. hyperboreus)*. Since the Arctic species are generally capital breeders, i.e. they reproduce before the onset of the bloom, the low densities of *Calanus*, and later developmental stages in particular, may well be due to post-reproductive, but pre-bloom, mortality.

The third possible mechanism is delayed advection of juvenile copepods into the Barents Sea from the Norwegian Sea. Ingvaldsen et al. (2002), however, did not find a distinct seasonal pattern in the inflow of Atlantic Water through the Barents Sea opening, and Skjoldal et al. (2021) did not observe a clear influence of varying inflow (advection) on interannual variation in *C. finmarchicus* abundance in the southern Barents Sea. Reproductive cycles of grazing copepods in the Norwegian Sea, which peak between mid-March and early May near the Barents Sea opening, result in seasonal advection of young stages into the Barents Sea by early summer (Skjoldal et al. 2021). In addition, the spring generation of *C. finmarchicus* is more abundant early in the season near the mainland coast and takes over a month to spread to 73.5° N (Skjoldal et al. 2021). Late-stage overwintering *Calanus* observed by these authors, however, were rarely found in our study, even at our most

southern station where CIs dominated. This pattern appeared to continue well into June as evidenced by our Sailbuoy data in the region, a finding consistent with a study from the same region that found secondary production dominated by nauplii and young developmental stages of *Calanus* only in late June (Gawinski et al. 2024).

4.3. Transfer of bloom carbon to planktivorous fish

Regardless of the mechanism(s), it is clear that low zooplankton abundances led to an unprecedented accumulation of phytoplankton biomass in our study region during spring blooms in two consecutive years. The consequences of this are substantial as mesozooplankton, and *Calanus* spp. copepods in particular, play an important role in the transfer of new production up the food chain.

Capelin is one of the most important planktivorous fish in boreal and sub-Arctic ecosystems. They play a critical role in maintaining commercial fish stocks (Koen-Alonso et al. 2021), but lack of sufficient prey can severely limit populations (Obradovich et al. 2014, Murphy et al. 2018). Once they are over approximately 7 cm in length (medium and large specimens in this study), they switch to diets consisting primarily of copepods and euphausiids (Eriksen et al. 2020).

Although capelin schools were frequently encountered south of the Polar Front, we found poor feeding by fish under 12 cm. Near the front, euphausiids were more abundant and both capelin and polar cod were feeding well on these, even if copepods were still in low density. Capelin are known to feed throughout the year when prey is present (Vesin et al. 1981). Whereas low light conditions in winter may reduce predation success, especially when prey density is low, light during our May study was high and lasted 24 h d^{-1}. Although there were reasonably high numbers of small copepods (e.g. *Oithona* spp.) in the plankton, these were only rarely observed in stomach samples. Predation on nauplii and small copepods, however, is not sufficient to compensate for lack of larger copepods and euphausiids in their diets (Grønkjær et al. 2019).

The capelin collected and detected acoustically in this study are likely juveniles and non-reproductive adults because adults spawn along the northern coast of mainland Norway and Russia at this time of year (Fall et al. 2023). Whereas the Polar Front appears to act as a (thermal) barrier for movement of capelin, a boreal species, to the northern Barents Sea where lipid-rich copepods (Wold et al. 2023) and euphausiids were more abundant, polar cod, an Arctic species, moved freely across the Front into the southern Barents Sea. These fish never had empty stomachs and may represent an effective competitor of capelin for the little prey available at this time of year.

The interactions among food availability, climatic conditions, and biological interactions have been extensively studied in Barents Sea capelin (Dolgov 2002, Gjøsæter et al. 2002, Orlova et al. 2009, 2010, 2013; Hop and Gjøsæter 2013), but few studies have taken place in early spring. Climatic conditions act in a complex manner in their influence on capelin feeding and nutrition as they differentially impact ice seasonality, bloom dynamics, and duration of copepod reproduction period (Orlova et al. 2010). Our results contribute to the understanding of this complexity, but also raise questions as to the consequences of the observed trophic disconnect during the spring period of high system productivity.

4.4. Insights from remote sensing

Remote sensing via satellites, unmanned Earth-based vehicles, and moored instruments have revolutionized data collection, visualization, and analysis of marineenvironmental and biological data. These tools have broadened the temporal and spatial range of data collected and provide broad multidisciplinary contextualization of the sampled parameters. Several large remote-sensing data services, e.g. the Copernicus system from the European Union's Space program, contain vast amounts of remotely sampled data and associated data products freely available to the public. One area where remote sensing has contributed considerably is in detecting changes in Arctic marine ecosystems, including sea-ice-cover change and its impacts on primary production (Arrigo et al. 2008, Kahru et al. 2011, Kahru et al. 2016, Bélanger et al. 2013, Ardyna and Arrigo 2020). A persistent issue, however, is that ice cover and clouds inhibit the detection of both ice-algal and under-ice algal concentrations. Where nutrient content is high, such as on Arctic continental shelves, estimates based on satellite imagery can underestimate annual primary production by as much as a factor of 10 (Arrigo et al. 2014).

Our extremely high Chl *a* biomass estimates in areas covered by sea ice support this contention, and Chl *a* biomass estimates from Copernicus for these stations predicted zero values instead of the high values we measured. Sea-ice conditions in the Barents Sea during winter (October-May) are strongly influenced by local winds that control ice import, both from the Arctic Ocean and the Laptev Sea (Efstathiou et al. 2022). A general reduction in ice cover in the region may make ice more mobile and, at least in the short term, increase periodic import of sea ice, making satellite detection of primary production challenging throughout the region.

We used the autonomous Sailbuoy platform equipped with an echosounder to investigate zooplankton populations in the region during and after shipboard operations in the Polar Front region. Data from this platform confirmed that meso- and macro- zooplankton populations were low for both an extended period of time and over a broad area exceeding that measured while the research vessel was on site. Backscatter profiles do not unequivocally identify the species responsible, but when coupled with net sampling and knowledge of the system, we can make reasonable assumptions the backscatter at a nominal frequency of 200 kHz was dominated by macro-and mesozooplankton. These additional observations are critical for contextualizing our findings and interpreting their potential ecosystem consequences.

4.5. Ecosystem consequences

Consequences of an extreme mismatch between primary productivity and presence of grazing zooplankton in the photic zone can have strong impacts on both food-web structure and, ultimately, the fate of new production. Without zooplankton to consume the bloom carbon, we expect a strong vertical flux of high-quality organic carbon to the seafloor (cf Arrigo et al. 2012), strengthening pelagic-benthic coupling. Indirect evidence for this comes from two sources. The high Chl *a* concentrations were observed to 50, 100, or even 200 m depth at multiple stations in our two surveys. In addition, Bodur et al. (2023) detected vertical carbon flux (>600 mg m^{-2} d^{-2}) with no attenuation in the export signal at one of our 2021 stations (M21_S5 at 76° N) just 2 weeks prior to our sampling. Unfortunately, we did not measure vertical carbon flux during our expedition, but this is the station where we saw a 16-fold increase in total integrated Chl *a* between samplings 2 weeks apart, suggesting that flux would have been even higher during our sampling campaign.

The presence of young *Calanus* copepodites, particularly in cold Polar Water north of the Polar Front, suggests that the bloom may not be entirely "wasted" for pelagic food-web connections. Rather at least the *Calanus* population in Arctic waters north of the Polar Front had timed their reproduction to match the development of the young recruits with the spring bloom. 75 % of *Calanus* had green guts in May 2022 (Daase, pers. observation) suggesting that those that were present did utilize the bloom. *Calanus* abundance observed by Wold et al. (2023) in July 2021 were 13–60 times higher than in May suggesting an overall successful recruitment. Despite this, the low densities of strong grazers at nearly all studies resulted in both a dramatic accumulation of phytoplankton biomass in the water column and a decoupling of the pelagic trophic links from phytoplankton for planktivorous fish.

Longer-term (decadal) projections for sea-ice cover in the Barents Sea suggest the region will go from a seasonally ice-covered area toa continuously ice-free by the end of this century, and perhaps as early as

2050 (Årthun et al. 2021). Pronounced interannual variability in ice cover during this transition period (Rieke et al. 2023), however, could lead to periods of increasing trends in sea-ice cover in the region, and perhaps more under-ice bloom beneath mobile and thinner ice (Ardyna et al., 2020). Chlorophyll *a* measurements conducted in the Barents Sea over the last 4 decades have shown a general increase that is related to reduced ice-cover and increased seawater temperatures (Dvoretsky et al. 2023). Models of changing ice phenology suggest earlier phytoplankton blooms (Manizza et al. 2023) and perhaps enhanced mismatch with consumers. In the Chukchi Sea, under-ice algal blooms accounted for 50 % of net primary productivity between 1988–2018, and years with high under-rice blooms exhibited increased mismatch between primary production and zooplankton grazing (Payne et al. 2021). Further, increased advection from the Pacific in this region increases the proportion of boreal planktonic species and, potentially, reductions in export of photosynthetic carbon to seafloor communities (Kędra et al., 2015).

Altered bloom phenology and increased mismatch can impact spawning and recruitment success in both herbivorous copepods (Søreide et al. 2010) and pelagic fish stocks (Asch et al. 2019). These events, even if relatively constrained in time, may have significant impacts on system functioning where multi-year lag times (Fransner et al. 2023) and dominance of specific year-classes (Ottersen and Loeng 2000, Planque et al. 2012) can drive primary and secondary productivity patterns over long periods, and impact ecosystem structure and carbon pathways.

CRediT authorship contribution statement

Paul E. Renaud: . **Malin Daase:** Writing – review & editing, Writing – original draft, Visualization, Methodology, Investigation, Funding acquisition, Formal analysis, Conceptualization. **Eva Leu:** Writing – review & editing, Writing – original draft, Supervision, Methodology, Investigation, Formal analysis, Conceptualization. **Maxime Geoffroy:** Writing – original draft, Visualization, Supervision, Methodology, Investigation, Formal analysis, Conceptualization. **Sünnje Basedow:** Writing – review & editing, Visualization, Supervision, Methodology, Investigation, Formal analysis, Conceptualization. **Mark Inall:** Writing – original draft, Visualization, Investigation, Formal analysis. **Karley Campbell:** Writing – review & editing, Supervision, Methodology. **Emilia Trudnowska:** Writing – review & editing, Writing – original draft, Visualization, Methodology, Investigation, Formal analysis, Conceptualization. **Einat Sandbank:** Writing – review & editing, Visualization, Methodology, Investigation, Formal analysis. **Frida Cnossen:** Writing – review & editing, Visualization, Investigation, Formal analysis. **Muriel Dunn:** Writing – review & editing, Writing – original draft, Visualization, Methodology, Investigation, Formal analysis. **Lionel Camus:** Writing – review & editing, Supervision, Methodology, Conceptualization. **Marie Porter:** Methodology, Conceptualization. **Magnus Aune:** Writing – review & editing, Methodology, Conceptualization. **Rolf Gradinger:** Writing – review & editing, Writing – original draft, Visualization, Methodology, Investigation, Formal analysis, Conceptualization.

Declaration of competing interest

The authors declare that they have no known competing financial interests or personal relationships that could have appeared to influence the work reported in this paper.

Acknowledgements

We are grateful for the efforts and skills of the captain and crew of the RV *Helmer Hanssen*. Funding for shiptime was provided by UiT The Arctic University of Norway via the ARCTOS Research Network. This study would not have been possible without technical expertise on land and at sea provided by C. Ballantine, H. Buschbaum, F. Cottier, J. Dörr, J. Gardner, E. Halvorsen, C. Helgeland, A. Miettinen, M. Lenss, V. Ramasco, and Y. Svensen. This project received funding from the Research Council of Norway (RCN #326635/E30 'PolarFront' and RCN #276730 'The Nansen Legacy'), with additional funding from Equinor, Conoco Philips, and the BioGlider project within the EU MarTERA program.

Appendix A. Supplementary material

Supplementary data to this article can be found online at https://doi.org/10.1016/j.pocean.2024.103365.

Data availability

DOIs for most data are listed in the article, some data are part of student theses and are embargoed

References

Arashkevich, E., Wassmann, P., Pasternak, A., Riser, C.W., 2002. Seasonal and spatial changes in biomass, structure, and development progress of the zooplankton community in the Barents Sea. J. Mar. Syst. 38, 125–145.
Ardyna, M., Arrigo, K.R., 2020. Phytoplankton dynamics in a changing Arctic Ocean. Nature Climate Ch 10, 892–903.
Arrigo, K.R., van Dijken, G., Pabi, S., 2008. Impact of a shrinking Arctic ice cover on marine primary production. Geophys. Res. Lett. 35, L19603.
Ardyna, M., Mundy, C.J., Mills, M.M., Oziel, L., Grondin, P.L., Lacour, L., Verin, G., Van Dijken, G., Ras, J., Alou-Font, E., Babin, M., 2020. Environmental drivers of under-ice phytoplankton bloom dynamics in the Arctic Ocean. Elem Sci Anth 8, 30.
Arrigo, K.R., Perovich, D.K., Pickart, R.S., Brown, Z.W., Van Dijken, G.L., Lowry, K.E., Mills, M.M., Palmer, M.A., Balch, W.M., Bahr, F., Bates, N.R., 2012. Massive phytoplankton blooms under Arctic sea ice. Science 336, 1408.
Arrigo, K.R., Perovich, D.K., Pickart, R.S., Brown, Z.W., Van Dijken, G.L., Lowry, K.E., Mills, M.M., Palmer, M.A., Balch, W.M., Bates, N.R., Benitez-Nelson, C.R., 2014. Phytoplankton blooms beneath the sea ice in the Chukchi Sea. Deep Sea Res II 105, 1–16.
Årthun, M., Onarheim, I.H., Dörr, J., Eldevik, T., 2021. The seasonal and regional transition to an ice-free Arctic. Geophys. Res. Lett. 48 e2020GL090825.
Asch, R.G., Stock, C.A., Sarmiento, J.L., 2019. Climate change impacts on mismatches between phytoplankton blooms and fish spawning phenology. Gl Ch Biol 25, 2544–2559.
Ashjian, C.J., Campbell, R.G., Welch, H.E., Butler, M., Van Keuren, D., 2003. Annual cycle in abundance, distribution, and size in relation to hydrography of important copepod species in the western Arctic Ocean. Deep-Sea Res. I 50, 1235–1261.
Balch, W.M., Bowler, B.C., Lubelczyk, L.C., Stevens Jr, M.W., 2014. Aerial extent, composition, bio-optics and biogeochemistry of a massive under-ice algal bloom in the Arctic. Deep-Sea Res. II 105, 42–58.
Basedow, S.L., McKee, D., Lefering, I., Gislason, A., Daase, M., Trudnowska, E., Egeland, E.S., Choquet, M., Falk-Petersen, S., 2019. Remote sensing of zooplankton swarms. Sci. Rep. 9, 1–10.
Bélanger, S., Babin, M., Tremblay, J.-É., 2013. Increasing cloudiness in Arctic damps the increase in phytoplankton primary production due to sea ice receding. Biogeosci 10, 4087–4101.
Blachowiak-Samolyk, K., 2008. Contrasting zooplankton communities (Arctic vs. Atlantic) in the European Arctic Marginal Ice Zone. Oceanologia 50, 363–389.
Bodur, Y.V., Renaud, P.E., Goraguer, L., Amargant-Arumí, M., Assmy, P., Dąbrowska, A. M., Marquardt, M., Renner, A.H., Tatarek, A., Reigstad, M., 2023. Seasonal patterns of vertical flux in the northwestern Barents Sea under Atlantic Water influence and sea-ice decline. Prog Oceanogr 219, 103132.
Camus, L., Andrade, H., Aniceto, A.S., Aune, M., Bandara, K., Basedow, S.L., Christensen, K.H., Cook, J., Daase, M., Dunlop, K., Falk-Petersen, S., Fietzek, P., Fonnes, G., Ghaffari, P., Gramvik, G., Graves, I., Hayes, D., Langeland, T., Lura, H., Kristiansen, T., Nøst, O.A., Peddie, D., Pederick, J., Pedersen, G., Sperrevik, A.K., Sørensen, K., Tassara, L., Tjøstheim, S., Tverberg, V., Dahle, S., 2021. Autonomous surface and underwater vehicles as effective ecosystem monitoring and research platforms in the Arctic – The GLIDER project. Sensors 21, 6752.
Chen, C.T., Millero, F.J., 1977. Speed of sound in seawater at high pressures. J. Acoust. Soc. Am. 62, 1129–1135.
Cnossen, F., 2022. Macrozooplankton distribution and feeding ecology of planktivorous fish at the Barents Sea Polar Front. MS Thesis, Université Côte d'Azur, Nice, France, 57 pp.
Coguiec, E., Last, K.S., Cohen, J.H., Hobbs, L., Choquet, M., Ershova, E., Berge, J., Daase, M., 2023. Photoperiodism and overwintering in boreal and sub-Arctic Calanus finmarchicus populations. Mar. Ecol. Prog. Ser. 712, 49–65.
Cushing, D.H., 1990. Plankton production and year-class strength in fish–populations – an update of the match mismatch hypothesis. Adv. Mar. Biol. 26, 249–293.
Dalpadado, P., Ingvaldsen, R., Hassel, A., 2003. Zooplankton biomass variation in relation to climatic conditions in the Barents Sea. Polar Biol. 26, 233–241.

Dalpadado, P., Yamaguchi, A., Ellertsen, B., Johannessen, S., 2008. Trophic interactions of macro-zooplankton (krill and amphipods) in the Marginal Ice Zone of the Barents Sea. Deep-Sea Res. II 55, 2266–2274.
Daase, M., Søreide, J.E., 2021. Seasonal variability in non-consumptive mortality of Arctic zooplankton. J Plankton Res 43, 565–585.
Daase, M., Varpe, Ø., Falk-Petersen, S., 2014. Non-consumptive mortality in copepods: occurrence of Calanus spp. carcasses in the Arctic Ocean during winter. J Plankton Res 36 (1), 129–144.
Dalpadado, P., Arrigo, K.R., van Dijken, G.L., Skjoldal, H.R., Bagøien, E., Dolgov, A.V., Prokopchuk, I.P., Sperfeld, E., 2020. Climate effects on temporal and spatial dynamics of phytoplankton and zooplankton in the Barents Sea. Prog. Oceanogr. 185, 102320. https://doi.org/10.1016/j.pocean.2020.102320.
Darnis, G., Fortier, L., 2014. Temperature, food and the seasonal vertical migration of key arctic copepods in the thermally stratified Amundsen Gulf (Beaufort Sea, Arctic Ocean). J. Plankton Res. 36, 1092–1108.
Darnis, G., Robert, D., Pomerleau, C., Link, H., Archambault, P., Nelson, R.J., Geoffroy, M., Tremblay, J.É., Lovejoy, C., Ferguson, S.H., Hunt, B.P., 2012. Current state and trends in Canadian Arctic marine ecosystems: II. Heterotrophic food web, pelagic-benthic coupling, and biodiversity. Clim Ch 115, 179–205.
de la Guardia, L.C., Fariñas, T.H., Marchese, C., Amargant-Arumí, M., Myers, P.G., Bélanger, S., Assmy, P., Gradinger, R., Duarte, P., 2023. Assessing net primary production in the northwestern Barents Sea using in situ, remote sensing and modelling approaches. Prog. Oceanogr. 219, 103160. https://doi.org/10.1016/j.pocean.2023.103160.
De Robertis, A., Higginbottom, I., 2007. A post-processing technique to estimate the signal-to-noise ratio and remove echosounder background noise. ICES J. Mar. Sci. 64, 1282–1291.
Demer, D.A., Berger, L., Bernasconi, M., Bethke, E., Boswell, K., Chu, D., Domokos, R., Dunford, A., Fässler, S., Gauthier, S. and Hufnagle, L.T. (2015) Calibration of acoustic instruments. ICES Cooperative Research Reports (CRR).
Dezutter, T., Lalande, C., Dufresne, C., Darnis, G., Fortier, L., 2019. Mismatch between microalgae and herbivorous copepods due to the record sea ice minimum extent of 2012 and the late sea ice break-up of 2013 in the Beaufort Sea. Prog. Oceanogr. 173, 66–77.
Dolgov, A.V., 2002. The role of capelin (*Mallotus villosus*) in the foodweb of the Barents Sea. ICES J. Mar. Sci. 59, 1034–1045.
Dong, K., Kvile, K.Ø., Stenseth, N.C., Stige, L.C., 2020. Associations among temperature, sea ice and phytoplankton bloom dynamics in the Barents Sea. Mar. Ecol. Prog. Ser. 635, 25–36. https://doi.org/10.3354/meps13218.
Dunn, M., Pedersen, G., Basedow, S.L., Daase, M., Falk-Petersen, S., Bachelot, L., Camus, L., Geoffroy, M., 2022. Inverse method applied to autonomous broadband hydroacoustic survey detects higher densities of zooplankton in near-surface aggregations than vessel-based net survey. Can. J. Fish. Aquat. Sci. 80, 451–467.
Dvoretsky, V.G., Vodopianova, V.V., Bulavina, A.S., 2023. Effects of climate change on chlorophyll a in the Barents Sea: a long-term assessment. Biology 12, 119. https://doi.org/10.3390/biology12010119.
Edvardsen, A., Slagstad, D., Tande, K.S., Jaccard, P., 2003a. Assessing zooplankton advection in the Barents Sea using underway measurements and modelling. Fish. Oceanogr. 12, 61–74.
Edvardsen, A., Tande, K.S., Slagstad, D., 2003b. The importance of advection on production of *Calanus finmarchicus* in the Atlantic part of the Barents Sea. Sarsia 88, 247–260.
Efstathiou, E., Eldevik, T., Årthun, M., Lind, S., 2022. Spatial patterns, mechanisms, and predictability of Barents Sea ice change. J. Clim. 35, 2961–2973.
Eiane, K. and Tande, K.S. (2009) Meso and microzooplankton. Ch 8 in: Sakshaug, E., Johnsen G., and Kovacs, K. (eds) Ecosystem Barents Sea. Tapir Academic Press, Trondheim Norway.
Eriksen, E., Benzik, A.N., Dolgov, A.V., Skjoldal, H.R., Vihtakari, M., Johannesen, E., Prokhorova, T.A., Keulder-Stenevik, F., Prokopchuk, I., Strand, E., 2020. Diet and trophic structure of fishes in the Barents Sea: The Norwegian-Russian program "Year of stomachs" 2015–Establishing a baseline. Prog. Oceanogr. 183, 102262.
Falk-Petersen, S., Hagen, W., Kattner, G., Clarke, A., Sargent, J., 2000. Lipids, trophic relationships, and biodiversity in Arctic and Antarctic krill. Can. J. Fish. Aquat. Sci. 57, 178–191.
Fall, J.J.E., Wenneck, T.D.L., Bogstad, B., Fuglebakk, E., Godiksen, J.A., Høines, Å.S., Korsbrekke, K., Skage, M.L., Staby, A., Tranang, C.A., Windsland, K., 2023. Fish investigations in the Barents Sea Winter 2022. IMR/PINRO Joint Rep Ser 2023.
Francois, R.E., Garrison, G.R., 1982. Sound absorption based on ocean measurements. Part I: Boric acid contribution and equation for total absorption. J Acoust Soc Amer 72, 1879–1890.
Fransner, F., Olsen, A., Årthun, M., Counillon, F., Tjiputra, J., Samuelsen, A., Keenlyside, N., 2023. Phytoplankton abundance in the Barents Sea is predictable up to five years in advance. Commun. Earth Environ. 4, 141.
Froese, R., Thorson, J.T., Reyes, R.B., 2014. A Bayesian approach for estimating length-weight relationships in fishes. J. Appl. Ichthyol. 30, 78–85.
Gawinski, C., Basedow, S.L., Sundfjord, A., Svensen, C., 2024. Secondary production at the Barents Sea polar front in summer is driven by small copepods and copepod nauplii. Mar. Ecol. Prog. Ser. 735, 77–101.
Gjøsæter, H., Dalpadado, P., Hassel, A., 2002. Growth of Barents Sea capelin (*Mallotus villosus*) in relation to zooplankton abundance. ICES J. Mar. Sci. 59, 959–967.
Głuchowska, M., Dalpadado, P., Beszczynska-Möller, A., Olszewska, A., Ingvaldsen, R.B., Kwasniewski, S., 2017. Interannual zooplankton variability in the main pathways of the Atlantic water flow into the Arctic Ocean (Fram Strait and Barents Sea branches). [ICES J Mar Sci, *74*, 1921-1936.Gradinger, R., 1996. Occurrence of an algal bloom under Arctic pack ice. Mar Ecol Prog Ser, *131*, 301-305].
Grønkjær, P., Nielsen, K.V., Zoccarato, G., Meire, L., Rysgaard, S., Hedeholm, R.B., 2019. Feeding ecology of capelin (*Mallotus villosus*) in a fjord impacted by glacial meltwater (Godthåbsfjord, Greenland). Polar Biol. 42, 81–98.
Hegseth, E.N., 1998. Primary production of the northern Barents Sea. Polar Res 17, 113–123.
Hop, H., Gjøsæter, H., 2013. Polar cod (*Boreogadus saida*) and capelin (*Mallotus villosus*) as key species in marine food webs of the Arctic and the Barents Sea. Mar. Biol. Res. 9, 878–894. https://doi.org/10.1080/17451000.2013.775458.
Huenerlage, K., Graeve, M., Buchholz, F., 2016. Lipid composition and trophic relationships of krill species in a high Arctic fjord. Polar Biol. 39, 1803–1817.
Hunt, G.L., Stabeno, P., Walters, G., Sinclair, E., Brodeur, R.D., Napp, J.M., Bond, N.A., 2002. Climate change and control of the southeastern Bering Sea pelagic ecosystem. Deep-Sea Res. II 49, 5821–5853.
Ingvaldsen, R.B., Assmann, K.M., Primicerio, R., Fossheim, M., Polyakov, I.V., Dolgov, A.V., 2021. Physical manifestations and ecological implications of Arctic Atlantification. Nat. Rev. Earth Environ. 2, 874–889. https://doi.org/10.1038/s43017-021-00228-x.
Ingvaldsen, R., Loeng, H., Asplin, L., 2002. Variability in the Atlantic inflow to the Barents Sea based on a one-year time series from moored current meters. Cont. Shelf Res. 22, 505–519.
Ji, R., Jin, M., Varpe, Ø., 2013. Sea ice phenology and timing of primary production pulses in the Arctic Ocean. Gl Ch Biol. 19, 734–741.
Kaartvedt, S., 2000. Life history of *Calanus finmarchicus* in the Norwegian Sea in relation to planktivorous fish. ICES J. Mar. Sci. 57, 1819–1824.
Kahru, M., Brotas, V., Manzano-Sarabiaz, M., Mitchell, B., 2011. Are phytoplankton blooms occurring earlier in the Arctic? Gl Ch Biol. 17, 1733–1739.
Kahru, M., Lee, Z.-P., Mitchell, B.G., Nevison, C.D., 2016. Effects of sea ice cover on satellite-detected primary production in the Arctic Ocean. Biol. Lett. 12, 20160223.
Kędra, M., Moritz, C., Choy, E.S., David, C., Degen, R., Duerksen, S., Ellingsen, I., Gorska, B., Grebmeier, J.M., Kirievskaya, D., van Oevelen, D., Piwosz, K., Samuelsen, A., Węsławski, J.M., 2015. Status and trends in the structure of Arctic benthic food webs. Polar Res. 34, 23775. https://doi.org/10.3402/polar.v34.23775.
Koen-Alonso, M., Lindstrøm, U., Cuff, A., 2021. Comparative modeling of cod-capelin dynamics in the Newfoundland-Labrador shelves and Barents Sea ecosystems. Front. Mar. Sci. 8, 579946.
Koenig, Z., Fer, I., Chierici, M., Fransson, A., Jones, E., Kolås, E.H., 2023. Diffusive and advective cross-frontal fluxes of inorganic nutrients and dissolved inorganic carbon in the Barents Sea in autumn. Prog. Oceanogr. 219, 103161.
Lawson, G.L., Barange, M., Fréon, P., 2001. Species identification of pelagic fish schools on the South African continental shelf using acoustic descriptors and ancillary information. ICES J. Mar. Sci. 58, 275–287.
Lien, V.S., 2018. Polarfrontens fysiske beskaffenhet og biologiske implikasjoner–en verdi- og sårbarhetsvurdering av polarfronten i Barentshavet. Fisken Havet 8-2018, 75 pp.
Madsen, S.D., Nielsen, T.G., Hansen, B.W., 2001. Annual population development and production by *Calanus finmarchicus, C. glacialis* and *C. hyperboreus* in Disko Bay, western Greenland. Mar. Biol. 139, 75–93.
Makarevich, P.R., Vodopianova, V.V., Bulavina, A.S., 2022. Dynamics of the spatial chlorophyll-a distribution at the Polar Front in the marginal ice zone of the Barents Sea during spring. Water 14, 101. https://doi.org/10.3390/w14010101.
Manizza, M., Carroll, D., Menemenlis, D., Zhang, H., Miller, C.E., 2023. Modeling the recent changes of phytoplankton blooms dynamics in the Arctic Ocean. e2022JC019152 J. Geophys. Res. Oceans 128. https://doi.org/10.1029/2022JC019152.
McNicholl, D.G., Walkusz, W., Davoren, G.K., Majewski, A.R., Reist, J.D., 2016. Dietary characteristics of co-occurring polar cod (*Boreogadus saida*) and capelin (*Mallotus villosus*) in the Canadian Arctic, Darnley Bay. Polar Biol. 39, 1099–1108.
Murphy, H.M., Pepin, P., Robert, D., 2018. Re-visiting the drivers of capelin recruitment in Newfoundland since 1991. Fish. Res. 200, 1–10.
Obradovich, S.G., Carruthers, E.H., Rose, G.A., 2014. Bottom-up limits to Newfoundland capelin (*Mallotus villosus*) rebuilding: the euphausiid hypothesis. ICES J. Mar. Sci. 71 (4), 775–783.
Orlova, E.L., Dolgov, A.V., Rudneva, G.B., Oganin, I.A., Konstantinova, L.L., 2009. Trophic relations of capelin *Mallotus villosus* and polar cod *Boreogadus saida* in the Barents Sea as a factor of impact on the ecosystem. Deep-Sea Res. II 56, 2054–2067.
Orlova, E.L., Rudneva, G.B., Renaud, P.E., Eiane, K., Savinov, V., Yurko, A.S., 2010. Climate impacts on feeding and condition of capelin *Mallotus villosus* in the Barents Sea: evidence and mechanisms from a 30 year data set. Aquat. Biol. 10, 105–118.
Orlova, E.L., Dolgov, A.V., Renaud, P.E., Boitsov, V.D., Prokopchuk, I.P., Zashihina, M.V., 2013. Structure of the macroplankton–pelagic fish–cod trophic complex in a warmer Barents Sea. Mar. Biol. Res. 9, 851–866.
Orlova, E.L., Dolgov, A.V., Renaud, P.E., Greenacre, M., Halsband, C., Ivshin, V.A., 2015. Climatic and ecological drivers of euphausiid community structure vary spatially in the Barents Sea: relationships from a long time series (1952–2009). Front. Mar. Sci. 1, 74. https://doi.org/10.3389/fmars.2014.00074.
Ottersen, G., Loeng, H., 2000. Covariability in early growth and year-class strength of Barents Sea cod, haddock, and herring: the environmental link. ICES J. Mar. Sci. 57, 339–348.
Oziel, L., Neukermans, G., Ardyna, M., Lancelot, C., Tison, J.-L., Wassmann, P., Sirven, J., Ruiz-Pino, D., Gascard, J.-C., 2017. Role for Atlantic Inflows and Sea Ice Loss on Shifting Phytoplankton Blooms in the Barents Sea. J. Geophys. Res. Oceans 122, 5121–5139.
Oziel, L., Massicotte, P., Randelhoff, A., Ferland, J., Vladoiu, A., Lacour, L., Galindo, V., Lambert-Girard, S., Dumont, D., Cuypers, Y., Bouruet-Aubertot, P., 2019. Environmental factors influencing the seasonal dynamics of spring algal blooms in

and beneath sea ice in western Baffin Bay. Elementa Sci Anthropocene 7, 34. https://doi.org/10.1525/elementa.372.
Parsons, T.R., Maita, Y., Lalli, C.M., 1984. Manual of Chemical and Biological Methods for Seawater Analysis. Pergamon Press, New York.
Payne, C.M., Bianucci, L., Van Dijken, G.L., Arrigo, K.R., 2021. Changes in under-ice primary production in the Chukchi Sea from 1988 to 2018. J Geophys Res: Oceans, 126, e2021JC017483.
Planque, B., Johannesen, E., Drevetnyak, K.V., Nedreaas, K.H., 2012. Historical variations in the year-class strength of beaked redfish (*Sebastes mentella*) in the Barents Sea. ICES J. Mar. Sci. 69, 547–552.
Planque, B., Primicerio, R., Michalsen, K., Aschan, M., Certain, G., Dalpadado, P., Gjøsæter, H., Hansen, C., Johannesen, E., Jørgensen, L.L., Kortsch, S., Leclerc, L., Omli, L., Skern-Mauritzen, M., Wiedmann, M., 2014. Who eats whom in the Barents Sea: a food web topology from plankton to whales. Ecol 95, 1430.
Polyakov, I.V., Pnyushkov, A.V., Alkire, M.B., Ashik, I.M., Baumann, T.M., Carmack, E. C., Goszczko, I., Guthrie, J., Ivanov, V.V., Kanzow, T., Krishfield, R., Kwok, R., Sundfjord, A., Morison, J., Rember, R., Yulin, A., 2017. Greater role of Atlantic inflows on sea-ice loss in the European Basin of the Arctic Ocean. Science 356, 285–291. https://doi.org/10.1126/science.aai8204.
Qu, B., Gabric, A.J., Matrai, P.A., 2005. The satellite-derived distribution of chlorophyll-a and its relation to ice cover, radiation and sea surface temperature in the Barents Sea. Polar Biol. 29, 196–210. https://doi.org/10.1007/s00300-005-0040-2.
Reigstad, M., Riser, C.W., Wassmann, P., Ratkova, T., 2008. Vertical export of particulate organic carbon: attenuation, composition and loss rates in the northern Barents Sea. Deep-Sea Res. II 55, 2308–2319.
Reigstad, M., Carroll, J., Slagstad, D., Ellingsen, I., Wassmann, P., 2011. Intra-regional comparison of productivity, carbon flux and ecosystem composition with the northern Barents Sea. Prog. Oceanogr. 90, 33–46.
Rieke, O., Årthun, M., Dörr, J.S., 2023. Rapid sea ice changes in the future Barents Sea. Cryosphere 17, 1445–1456.
Ryan, T.E., Downie, R.A., Kloser, R.J., Keith, G., 2015. Reducing bias due to noise and attenuation in open-ocean echo integration data. ICES J. Mar. Sci. 72, 2482–2493.
Samemoto, D.D., 1987. Vertical distribution and ecological significance of chaetognaths in the Arctic environment of Baffin Bay. Polar Biol. 7, 317–328.
Skjoldal, H.R., Aarflot, J.M., Bagøien, E., Skagseth, Ø., Rønning, J., Lien, V.S., 2021. Seasonal and interannual variability in abundance and population development of Calanus finmarchicus at the western entrance to the Barents Sea, 1995–2019. Prog. Oceanogr. 195, 102574.
Søreide, J.E., Dmoch, K., Blachowiak-Samolyk, K., Trudnowska, E., Daase, M., 2022. Seasonal mesozooplankton patterns and timing of life history events in high-arctic fjord environments. Front Mar Sci 9, 933461.
Søreide, J.E., Leu, E., Berge, J., Graeve, M., Falk-Petersen, S., 2010. Timing of blooms, algal food quality and *Calanus glacialis* reproduction and growth in a changing Arctic. Gl Ch Biol 16, 3154–3163. https://doi.org/10.1111/j.1365-2486.2010.02175.x.
Sundfjord, A., Assmann, K.M., Lundesgaard, Ø., Renner, A.H., Lind, S., Ingvaldsen, R.B., 2020. Suggested water mass definitions for the central and northern Barents Sea, and the adjacent Nansen Basin: Workshop Report. The Nansen Legacy Report Series, 8.
Sverdrup, H., 1953. On conditions for the vernal blooming of phytoplankton. J Cons/cons Perm Int L'explor Mer 18, 287–295.
Swalethorp, R., Kjellerup, S., Dünweber, M., Nielsen, T.G., Møller, E.F., Rysgaard, S., Hansen, B.W., 2011. Grazing, egg production, and biochemical evidence of differences in the life strategies of *Calanus finmarchicus, C. glacialis* and *C. hyperboreus* in Disko Bay, western Greenland. Mar. Ecol. Prog. Ser. 429, 125–144.
Tande, K.S., 1991. *Calanus* in North Norwegian fjords and in the Barents Sea. Polar Res. 10, 389–407.
Terazaki, M., 2004. Life history strategy of the chaetognath Sagitta elegans in the worlds' oceans. Coast Mar Sci 29, 1–12.
Toresen, R., Gjøsæter, H., de Barros, P., 1998. The acoustic method as used in the abundance estimation of capelin (*Mallotus villosus* Müller) and herring (*Clupea harengus* Linné) in the Barents Sea. Fish. Res. 34, 27–37. https://doi.org/10.1016/S0165-7836(97)00077-5.
Trudnowska, E., Głuchowska, M., Beszczynska-Möller, A., Błachowiak-Samołyk, K., Kwasniewski, S., 2016. Plankton patchiness in the Polar Front region of the West Spitsbergen Shelf. Mar. Ecol. Prog. Ser. 560, 1–18.
Vesin, J.P., Leggett, W.C., Able, K.W., 1981. Feeding ecology of capelin (*Mallotus villosus*) in the estuary and western Gulf of St. Lawrence and its multispecies implications. Canadian J Fish Aquat Sci 38, 257–267.
Walkusz, W., Kwasniewski, S., Falk-Petersen, S., Hop, H., Tverberg, V., Wieczorek, P., Węsławski, J.M., 2009. Seasonal and spatial changes in the zooplankton community of Kongsfjorden, Svalbard. Polar Res. 28, 254–281.
Wassmann, P., Ratkova, T., Andreassen, I., Vernet, M., Pedersen, G., Rey, F., 1999. Spring Bloom Development in the Marginal Ice Zone and the Central Barents Sea. Mar. Ecol. 20, 321–346. https://doi.org/10.1046/j.1439-0485.1999.2034081.x.
Wassmann, P., Reigstad, M., 2011. Future Arctic Ocean seasonal ice zones and implications for pelagic-benthic coupling. Oceanogr 24, 220–231. https://doi.org/10.5670/oceanog.2011.74.
Wassmann, P., Reigstad, M., Haug, T., Rudels, B., Carroll, M.L., Hop, H., Gabrielsen, G. W., Falk-Petersen, S., Denisenko, S.G., Arashkevich, E., Slagstad, D., 2006. Food webs and carbon flux in the Barents Sea. Prog. Oceanogr. 71, 232–287.
Wold, A., Hop, H., Svensen, C., Søreide, J.E., Assmann, K.M., Ormanczyk, M., Kwasniewski, S., 2023. Atlantification influences zooplankton communities seasonally in the northern Barents Sea and Arctic Ocean. Prog. Oceanogr. 219, 103133.